^{14}N and ^{81}Br Quadrupolar Nuclei as Sensitive NMR Probes of *n*-Alkyltrimethylammonium Bromide Crystal Structures. An Experimental and Theoretical Study

Bruno Alonso,*,† Dominique Massiot,‡ Pierre Florian,‡ Henrich H. Paradies,§ Philippe Gaveau,† and Tzonka Mineva†

Institut Charles Gerhardt de Montpellier, Matériaux Avancés pour la Catalyse et la Santé, ICGM-MACS, UMR 5253 CNRS-ENSCM-UM2-UM1, 8 rue de l'Ecole Normale, 34296 Montpellier cedex 5, France, CEMHTI, CNRS UPR3079 Université d'Orléans, 1D av. de la Recherche Scientifique, 45071 Orléans cedex 2, France, and The University of Salford, Joule Physics Laboratory, School of Computing, Science and Engineering, Materials Research Institute, Manchester, M 5 4WT, United Kingdom

Received: March 27, 2009; Revised Manuscript Received: July 6, 2009

This is the first time a comprehensive study has been carried out on *n*-alkyltrimethylammonium bromide salts using ^{14}N and ^{81}Br solid state NMR, X-ray diffraction, and theoretical calculations. The investigation represents a necessary step toward further ^{14}N and ^{81}Br NMR characterization of the environment of cationic and anionic groups in materials, accounting for the amphiphilic properties of cationic surfactants. The NMR spectra of five $C_xH_{2x+1}(CH_3)_3N^+Br^-$ polycrystalline samples with different *n*-alkyl chain lengths (x = 1, 12, 14, 16, 18) were recorded and modeled. The ^{14}N and ^{81}Br quadrupolar coupling interaction parameters (C_Q, η_Q) were also estimated from spectrum modeling and from computer simulation. The obtained results were discussed in depth making use of the experimental and reoptimized crystal structures. In the study, both ^{14}N and ^{81}Br nuclei were found to be sensitive probes for small structural variations. The parameters which influence the NMR properties the most are mobility, deviation of C−N−C bond angles from T_d angles, and variations in r(N−Br) distances.

I. Introduction

Because of their amphiphilic properties, quaternary ammonium salts are widely used in various applications, e.g., detergents, textile softeners, household materials, liquid crystals, and processed materials.[1,2] In particular, the single chained *n*-alkyltrimethylammonium bromide salts have been successfully employed in the synthesis of new inorganic mesoporous materials using cationic surfactants as templates.[3,4] Since this seminal discovery, continuous efforts have been devoted toward the combination of soft chemistry and self-assembly processes, and by stimulating considerable interest in their structure, properties, formation mechanisms, and possible applications.[5−9] The significance of the interactions between the positively charged headgroup, the counteranions, and other chemical and/or physical entities, e.g., size and shape polydispersity of the apparent aggregates, nature of the solvent, and effective colloidal charges, have also been highlighted.[10−20] NMR of ^{14}N, $^{79/81}$Br, or $^{35/37}$Cl nuclei would be a very informative technique for the characterization of both physical and chemical properties of these cationic amphiphiles in various dispersions. Nevertheless, very little is known with respect to the relation to the ^{14}N NMR analysis of the formation of the materials[21−23] and even less for the final materials.[24] Similarly, nothing has been reported to our knowledge on the characterization of the counteranions Br^- or Cl^- using either $^{79/81}$Br or $^{35/37}$Cl NMR, probably because of the large quadrupolar coupling constants, C_Q. We believe that additional information can be gained by studying these and other materials through solid state NMR methods involving these abundant quadrupolar nuclei: ^{14}N (I = 1, 99.6% abund.) on one side which is representative of the polar head groups and $^{79/81}$Br (I = 3/2, 50.7/49.3% abund.) or ^{35}Cl (I = 3/2, 75.8% abund.) on the other side, which are representatives of the counteranions. Therefore, our first experimental approach was to study the widely used polycrystalline *n*-alkyltrimethylammonium bromide salts $C_xH_{2x+1}(CH_3)_3N^+Br^-$ by means of ^{14}N and ^{81}Br solid state NMR which may exploit new ways for possible studies of more complex materials in the near future.

The characterization of solid samples by ^{14}N MAS NMR has been attracting more attention over the last 10 years,[25−27] facing the problem of large quadrupolar coupling constants C_Q encountered in the case of amino acid functionality. In parallel, different indirect methods (spin-$^1/_2$ detection) have been developed to estimate ^{14}N NMR interactions,[28−31] and very recently to record ^{14}N spectra.[32−34] Overtone ^{14}N NMR spectroscopy,[35−37] aiming at acquiring directly double quantum spectra, has been investigated by several groups over the last years but has not succeeded yet in reaching the required efficiency for their use in real material science applications. For tetraalkylammonium salts, only a few recent studies have been devoted to their detailed solid state ^{14}N MAS NMR characterization[38,39] which complete earlier data obtained under static conditions.[40,41] In the case of *n*-alkyltrimethylammonium bromide salts $C_xH_{2x+1}(CH_3)_3N^+Br^-$ with long chains (x > 4), ^{14}N static NMR studies have been published earlier for the hexadecyltrimethylammonium bromide (HTAB, x = 16) and decyltrimethylammonium bromide (x = 10).[41] In all of these studies, the values of the quadrupolar coupling constant C_Q were always small and significantly below 1 MHz, allowing a direct observation of ^{14}N using standard solid state NMR spectrometers.

In the case of solid state NMR characterization involving $^{79/81}$Br nuclei, there have been only a few reports published and

* Corresponding author. E-mail: bruno.alonso@enscm.fr. Phone: +33 (0)4 67 16 34 68. Fax: +33 (0)4 67 16 34 70.
† Institut Charles Gerhardt de Montpellier.
‡ Université d'Orléans.
§ The University of Salford.

10.1021/jp9027904 CCC: $40.75
Published on Web 08/12/2009

recently reviewed,[42] but virtually no information exists on *n*-alkyltrimethylammonium bromide salts. Nowadays, the access to high magnetic fields opens new opportunities for the characterization of materials by solid state NMR of half integer quadrupolar nuclei.[43] It thus becomes possible to characterize and explore the Br environment by solid state NMR.

The purpose of this contribution is to analyze by means of ^{14}N and ^{81}Br MAS NMR *n*-alkyltrimethylammonium bromide salts $C_xH_{2x+1}(CH_3)_3N^+Br^-$ with different alkyl chain lengths (x = 1, 12, 14, 16, 18) and to evaluate the effect of their structure on the NMR parameters using crystallographic data and theoretical calculations. Particular attention has been devoted to nuclear quadrupolar coupling interaction parameters which are highly informative and accessible from experiments and calculations.

II. Experimental Methods

II.1. Chemical Compounds. Tetramethylammonium bromide (TMAB, pur. ≥ 99%), dodecyltrimethylammonium bromide (DTAB, pur. ≥ 98%), tetradecyltrimethylammonium bromide (TTAB, pur. ≥ 99%), hexadecyltrimethylammonium bromide (HTAB, pur. ≥ 99%), and octadecyltrimethylammonium bromide (OTAB, pur. ≥ 97%) were used as purchased from Sigma-Aldrich. Before and after use, a single crystal phase is observed by XRD for these powdered compounds.

II.2. Solid State NMR. ***II.2.1. Spectrum Acquisition.*** ^{14}N NMR spectra were recorded at a Larmor frequency $\nu_0(^{14}N) \equiv 28.91$ MHz ($B_0 = 9.4$ T) on a widebore Varian Infinity 400 spectrometer using 7.5 mm zirconia rotors spun at ν_{MAS} ranging from 1 to 6 kHz. A single pulse sequence was employed with 18° pulse angles (RF field strength ∼25 kHz), 0.5 s of recycling delays, and ^{1}H decoupling during acquisition (RF field strength ∼50 kHz). For some compounds, ^{14}N NMR experiments were also performed at $\nu_0(^{14}N) \equiv 54.19$ MHz ($B_0 = 17.6$ T) on a widebore Bruker Avance 750 spectrometer using 4 mm rotors. ^{14}N chemical shifts are here referenced using $\delta_{iso} = 0$ ppm for the signal of solid NH_4Cl spun at $\nu_{MAS} = 5$ kHz, which is at −342.4 ppm relative to nitromethane.[26] ^{14}N spectra can be very sensitive to slightly off-MAS conditions.[26,44] The magic angle was set here so as to anneal the splitting of the TMAB center band, as done with other compounds in previous works.[26] It has been verified that the spinning sideband pattern (SSB) does not change when varying the irradiation frequency (50 kHz offset).

Complementary ^{15}N{^{1}H} cross-polarization (CP) MAS spectra were recorded at a Larmor frequency $\nu_0(^{15}N) \equiv 40.55$ MHz ($B_0 = 9.4$ T) on a widebore Varian Infinity spectrometer using 7.5 mm zirconia rotors spun at ν_{MAS} ranging from 0.5 to 1 kHz. The conditions used are similar to those published earlier.[38] The CP contact time was fixed to 3 ms, and RF field strengths were about 50 kHz.

^{81}Br NMR spectra were recorded at $\nu_0(^{81}Br) \equiv 202.60$ MHz ($B_0 = 17.6$ T) on a widebore Bruker Avance 750 spectrometer using 2.5 and 4 mm zirconia rotors spun at ν_{MAS} ranging from 0 to 30 kHz. ^{81}Br spectra were recorded using Hahn echoes: 45° pulse−τ−90° pulse−τ−Acq., where τ is synchronized with MAS and in the range (33−143) × 10^{-6} s, and using a RF field strength of 50 kHz. For the highest ν_{MAS}, it has been verified that the single pulse spectra yielded the same results. ^{1}H decoupling during acquisition (RF field strength ∼50 kHz) was only used for static conditions. We have also verified that no ^{1}H decoupling during acquisition was necessary during the acquisition of ^{81}Br signals for the rotating samples ($\nu_{MAS} \geq 7$ kHz). Here, ν_{MAS} are almost 3 times the values of the more intense

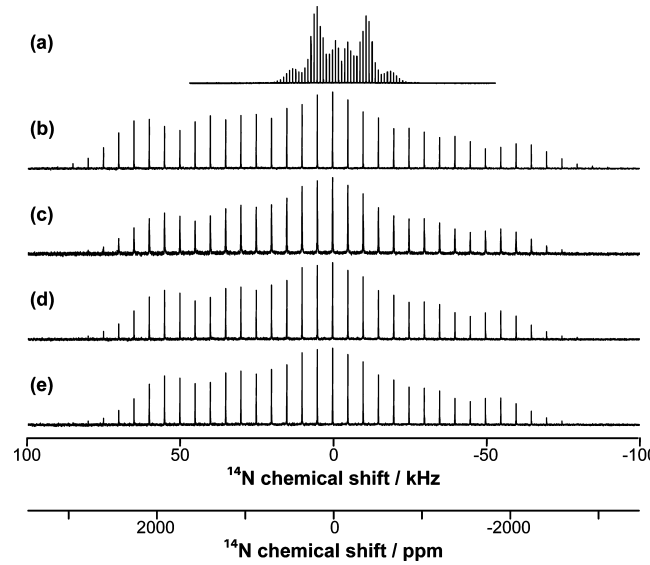

Figure 1. ^{14}N spectra ($B_0 = 9.4$ T; $\nu_0 \equiv 28.91$ MHz) of *n*-alkyltrimethylammonium bromide salts $C_xH_{2x+1}(CH_3)_3N^+Br^-$: (a) TMAB ($x = 1$), (b) DTAB ($x = 12$), (c) TTAB ($x = 14$), (d) HTAB ($x = 16$), (e) OTAB ($x = 18$). The MAS frequency ν_{MAS} was fixed to (a) 1 kHz or (b−e) 5 kHz.

^{81}Br−^{1}H dipolar couplings (<2 kHz) estimated from the Br−H distances found in the crystal structure of HTAB.[45] Recycle delays were kept low (between 0.3 and 1 s) and no significant loss of signals was noticed. The chemical shift reference used here ($\delta_{iso} = 0$ ppm) is solid KBr spun at a moderate frequency (about 2−5 kHz).

II.2.2. Convention for NMR Interactions. The nuclear quadrupolar coupling (QUAD) interaction tensor is described by the quadrupolar coupling constant C_Q and the asymmetry parameter η_Q defined by the principal values V_{ii} of the electric field gradient tensor (EFG) following

$$C_Q = eQV_{33}/h; \eta_Q = (V_{22} - V_{11})/V_{33}$$

where $V_{33} = eq$, $V_{33} + V_{22} + V_{11} = 0$, and $|V_{33}| > |V_{11}| > |V_{22}|$.

Following Haeberlen notations and IUPAC recommendations,[46] the chemical shift anisotropy (CSA) interaction tensor is defined by the isotropic chemical shift δ_{iso}, the anisotropy Δ_{CSA}, and the asymmetry η_{CSA} parameters. These parameters are defined here by

$$\delta_{iso} = (\delta_{11} + \delta_{22} + \delta_{33})/3; \Delta_{CSA} = (\delta_{33} - \delta_{iso}); \eta_{CSA} = (\delta_{22} - \delta_{11})/(\delta_{33} - \delta_{iso})$$

where $|\delta_{33} - \delta_{iso}| > |\delta_{11} - \delta_{iso}| > |\delta_{22} - \delta_{iso}|$.

The Euler angles (ϕ, χ, ψ) describe the orientation of the CSA tensor with respect to the EFG tensor. In the case of powders, the angle intervals can be restricted[47,48] and we used same common intervals as in SIMPSON software.[49]

II.2.3. Spectrum Modeling. Spectra were modeled using the DmFit software[50] freely accessible from the Internet.[51] For both ^{14}N and ^{81}Br spectra, the model function denoted "*Int2Quad*" in the DmFit software was employed. This model assumes ideal excitation and detection and takes into account the quadrupolar and CSA interactions, with their Euler angles and the effect of the MAS spinning rate. The related NMR parameters can be fixed or estimated from an iterative fitting procedure, following previous analysis and fitting procedures.[52] More details about

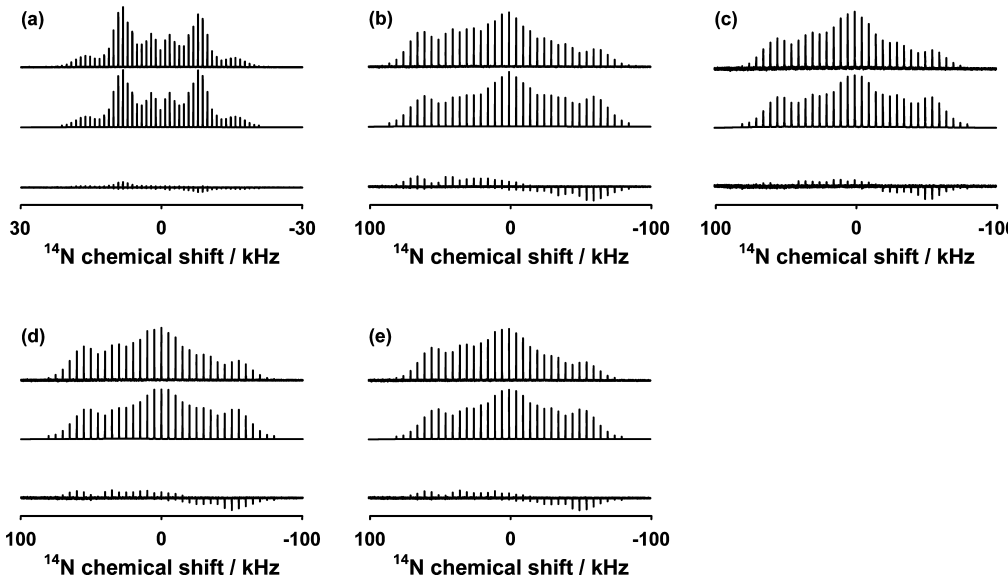

Figure 2. Modeling of ^{14}N spectra: (a) TMAB ($x = 1$), (b) DTAB ($x = 12$), (c) TTAB ($x = 14$), (d) HTAB ($x = 16$), (e) OTAB ($x = 18$). For each sample, the experimental spectrum is shown at the top, the model in the middle, and the difference between both of them at the bottom. The spectra and acquisition conditions are the same as those in Figure 1.

TABLE 1: ^{14}N NMR Parameters of *n*-Alkyltrimethylammonium Bromide Salts $C_xH_{2x+1}(CH_3)_3N^+Br^-$ from Previous Works and This Work[a]

crystal salt	δ_{iso}[b] (ppm)	C_Q (kHz)	η_Q	$\nu(^{14}N)$ (MHz)	ν_{MAS} (kHz)	T/K	ref
TMAB ($x = 1$)	9.2	26.2	0.04	28.9	1	~293	this work
id		26.5		26	0	296	ref 40
id		26.6 ± 0.2	0.00 ± 0.02	19.5	0	290	ref 41
id		25.2	0.0	21.7	0	293	ref 86
dTAB ($x = 10$)		116.0 ± 1.0	0.85 ± 0.02	19.5	0	293	ref 41
DTAB ($x = 12$)	13.0	107.2	0.90	28.9	5	~293	this work
TTAB ($x = 14$)	13.0	97.4	0.90	28.9	5	~293	this work
HTAB ($x = 16$)	13.0	97.8	0.84	28.9	5	~293	this work
id		98.0 ± 1.0	0.90 ± 0.02	19.5	0	293	ref 41
OTAB ($x = 18$)	13.0	96.9	0.84	28.9	5	~293	this work

[a] Unless otherwise reported, the errors bars are of ±0.2 ppm for δ_{iso}, ±1 kHz for C_Q, and ±0.01 for η_Q. [b] Relative to NH_4Cl span at 4 kHz.

the use of the fitting procedures are presented in the Results section. The DmFit program has been modified so as to estimate mathematical fitting errors from covariance matrix and/or Monte Carlo analysis.[53−55] They correspond to a 95% confidence limit.

II.2.4. Theoretical Calculations. Optimized geometrical parameters and EFG of TMAX (X ≡ Cl, Br, I), NH_4Cl, and HTAB bulk structures were computed in the frame of the periodic density functional (DF) approach with the Crystal 06 computer package.[56] The calculations were carried out at $T = 0$ K. Therefore, only the low temperature phase (symmetry *P4*/*nmm* space group) which is common for the three TMAX salts was considered, though different unit cell parameters or even crystal phases at various temperatures and degrees of hydration have been proposed.[57−59] However, for the present study, the most detailed TMAB crystal structure data set was taken from ref 59, and for TMAC and TMAI, the published values of Wyckoff for the *a* and *c* lattice vectors were used.[57] The initial structural parameters of the HTAB $P2_1$ unit cell are those of polymorph III,[45] which are very close to our XRD results.

The atomic positions in the TMAX, HTAB, and reference NH_4Cl unit cells were fully optimized employing the B3LYP[60,61] approximation for the exchange-correlation functional. The basis set of double-ζ quality (6-31d1)[62] was used to describe N, C, and H atoms; the Cl, Br, and I atoms were described with the HAYWLC[63] effective core potential basis set in the geometry optimization. EFG tensors in the principle axes of the compounds were computed for the optimized structures. EFG values at the Br nucleus in TMAB and HTAB crystals were obtained from single point energy calculations for the optimized geometry using all electron double-ζ basis, DZVP.[64]

EFG tensors were also computed for $[N(CH_3)_4X_8]^{7-}$ and $[N(CH_3)_4]^+$ clusters cut from the optimized bulk structures for the TMAX salts and centered at the N atom (see Figure 8b). These cluster calculations were carried out again with the B3LYP functional using g03 code.[65] Initial test calculations for the TMAB cluster were performed with the 6-311g(d,p),[66−68] IGLOIII,[69] and Aug-cc-pVTZ[70,71] basis sets. As the NMR property variation was less than 8%, the 6-311g(d,p) basis set was employed for the results presented in this work. Nuclear quadruple moments (eQ) of 26.2 and 2.04 Q/fm^2, respectively,[72] have been used for the ^{81}Br and ^{14}N C_Q calculations.

II.3. X-ray Methods. ***II.3.1. Powder Diffraction.*** XRD diffractograms at small angle were recorded in a conventional $\theta-\theta$ Bragg−Brentano configuration (Ni-filtered Cu Kα1,2 = 1.5418 Å) on a Bruker-AXS D8 Advance Powder X-ray diffractometer fitted with a linear Vantec-1 detector. The maximum lengths l_{max} of the fully extended $C_xH_{2x+1}(CH_3)_3N^+$ cations have been estimated using two different approximations: empirical values normally used in surfactant systems[73] and crude force field geometric optimization.[74] l_{max} values were used to

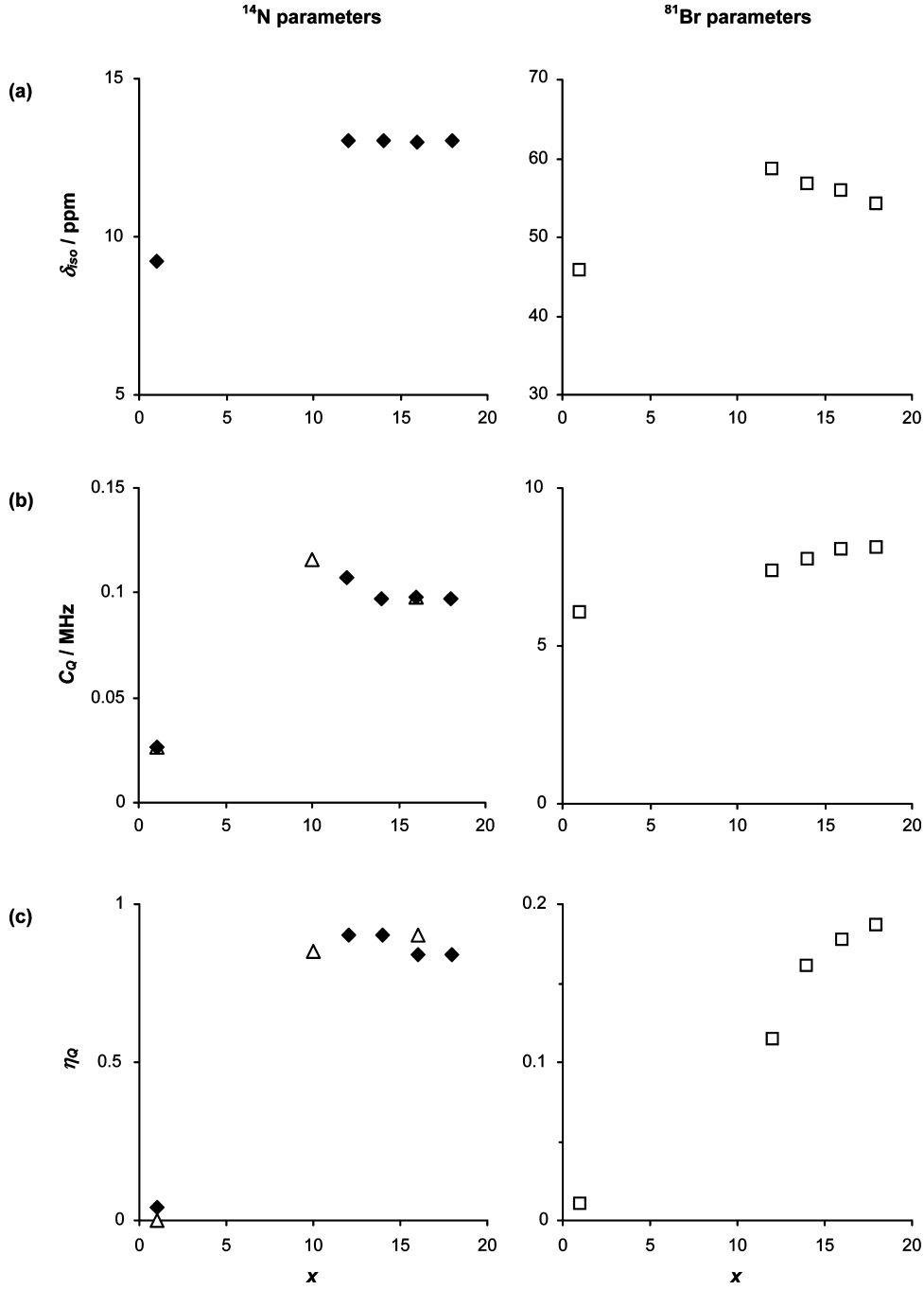

Figure 3. Variations of (a) δ_{iso}, (b) C_Q, and (c) η_Q parameters as a function of x for (♦) ^{14}N and (□) ^{81}Br modeled spectra of *n*-alkyltrimethylammonium bromide salts $C_xH_{2x+1}(CH_3)_3N^+Br^-$. For ^{14}N C_Q and η_Q parameters, (Δ) additional points are taken from ref 41.

estimate the maximum unit cell parameter c_{max} corresponding to ideal bilayers with perpendicular alkyl chains.

II.3.2. Crystal Structure Determination. The crystal structure of HTAB (polymorph III) used for calculations was determined from colorless plate-shaped crystal grown at 20−25 °C from purely organic solvents comprised of ether/ethylacetate (90/10%v/v), having approximate dimensions of 0.40 × 0.30 × 0.01 mm^3, and mounted on a glass fiber. Measurements were made on a Rigaku AFC5R diffractometer with graphic monochromatic Cu Kα radiation and a 12 KW rotating anode generator. More information (about experimental conditions, atomic coordinates, *U* values, intramolecular distances, and torsion or conformational angles) is available as Supporting Information (S1). The structures of polymorphs I, II, and III of HTAB are described elsewhere.[45]

III. Results

III.1. Experimental NMR Spectra and Modeling. ***III.1.1. ^{14}N.*** We have studied the following *n*-alkyltrimethylammonium bromide salts $C_xH_{2x+1}(CH_3)_3N^+Br^-$ by solid state ^{14}N MAS NMR: tetramethylammonium bromide (TMAB, x = 1), dodecyltrimethylammonium bromide (DTAB, x = 12), tetradecyltrimethylammonium bromide (TTAB, x = 14), hexadecyltrimethylammonium bromide (HTAB, x = 16), and octadecyltrimethylammonium bromide (OTAB, x = 18). Their ^{14}N MAS spectra recorded at B_0 = 9.4 T ($\nu_0 \equiv$ 28.91 MHz) are presented in Figure 1. The extent of the observed SSB mostly depends on the intensity of the quadrupolar coupling (QUAD) interaction. A static quadrupolar coupling, characterized by its intensity C_Q and its asymmetry parameter η_Q, gives rise at first

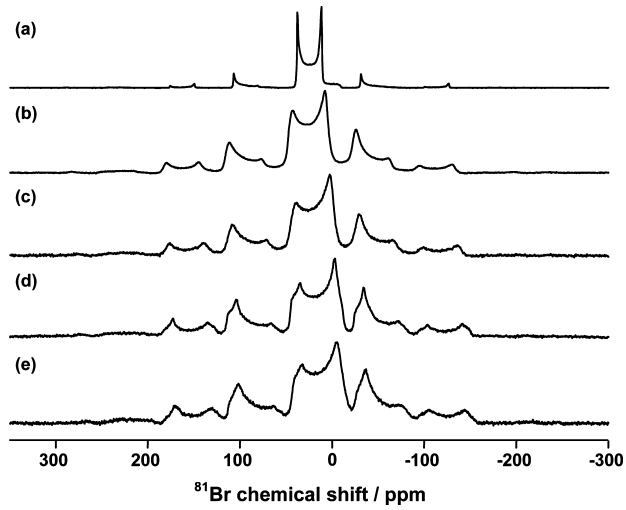

Figure 4. ^{81}Br spectra ($B_0 = 17.6$ T; $\nu_0 \equiv 202.60$ MHz, $\nu_{MAS} = 14$ kHz) of *n*-alkyltrimethylammonium bromide salts $C_xH_{2x+1}(CH_3)_3N^+Br^-$: (a) TMAB ($x = 1$), (b) DTAB ($x = 12$), (c) TTAB ($x = 14$), (d) HTAB ($x = 16$), (e) OTAB ($x = 18$).

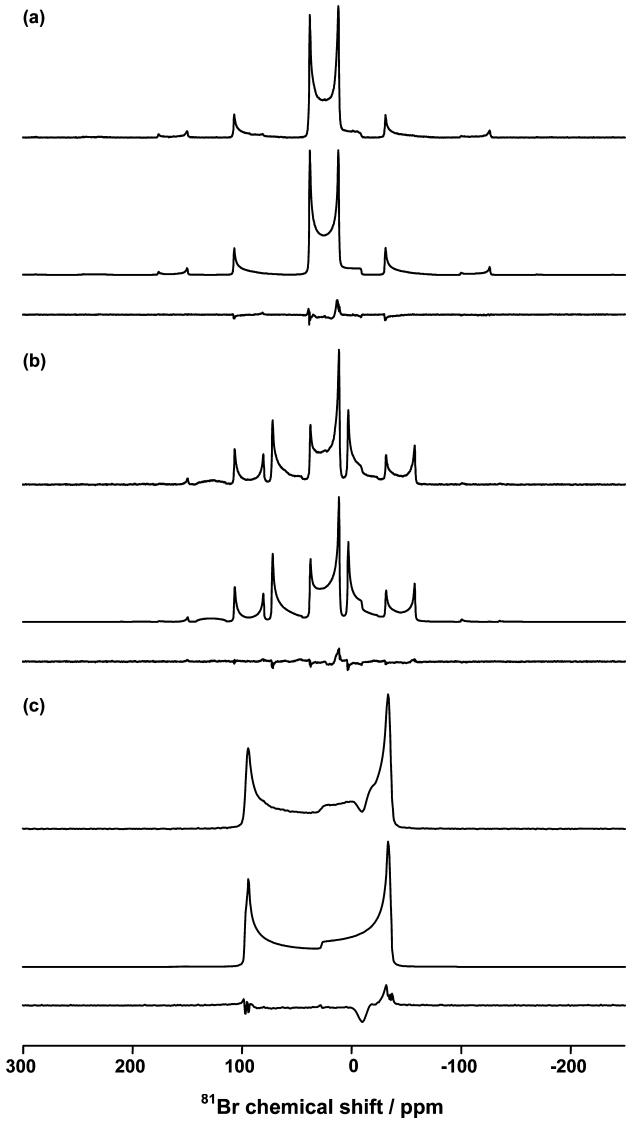

Figure 5. Modeling of ^{81}Br spectra of TMAB ($x = 1$): (a) $\nu_{MAS} = 14$ kHz, (b) $\nu_{MAS} = 7$ kHz, (c) $\nu_{MAS} = 0$ kHz. The experimental spectrum is shown at the top, the model in the middle, and the difference between both of them at the bottom.

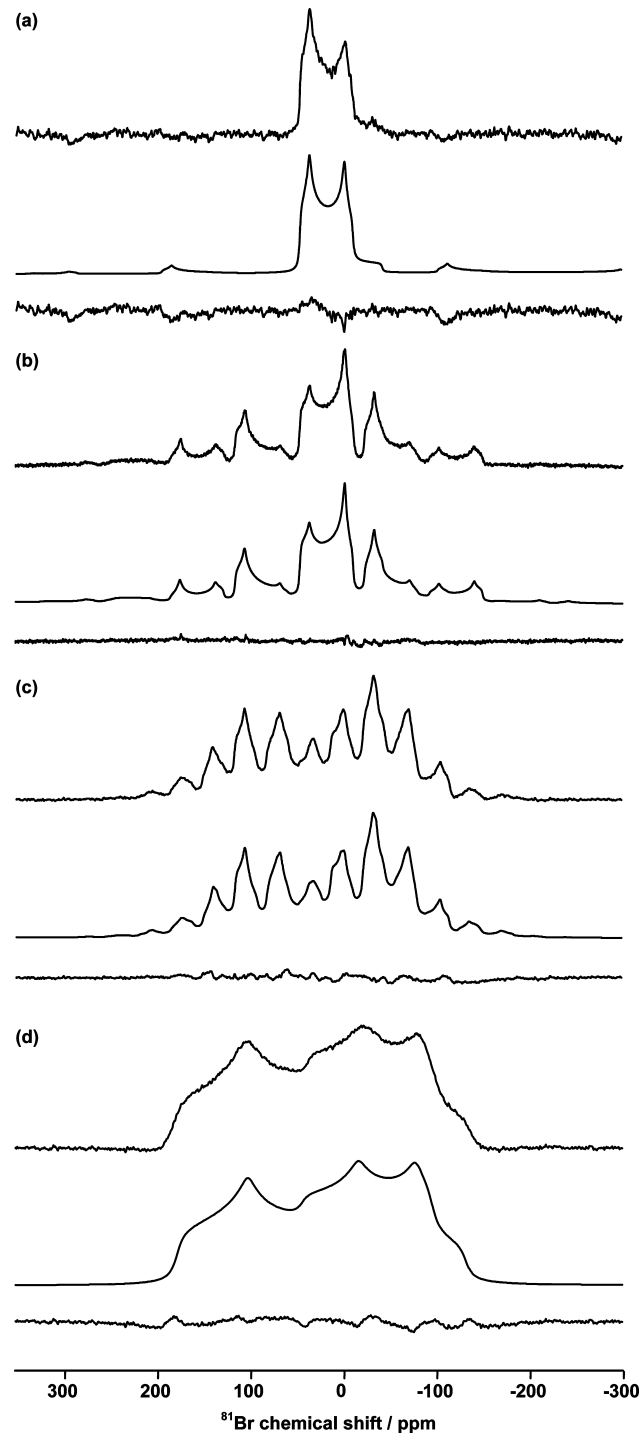

Figure 6. Modeling of ^{81}Br spectra of HTAB ($x = 16$): (a) $\nu_{MAS} = 30$ kHz, (b) $\nu_{MAS} = 14$ kHz, (c) $\nu_{MAS} = 7$ kHz, (d) $\nu_{MAS} = 0$ kHz. The experimental spectrum is shown at the top, the model in the middle, and the difference between both of them at the bottom.

order to a symmetric spinning sideband manifold whose sideband intensities allow measuring the interaction.[25−27,75] We have modeled these ^{14}N spectra by considering only the quadrupolar interaction. The results are presented in Figure 2 and summarized in Table 1. The differences between the experimental spectra and the models are small (Figure 2) but always nonsymmetrical. The chemical shift anisotropy (CSA) interaction, if significant, introduces an asymmetry of the spinning sideband intensities, as reported earlier for other nitrogen containing crystals.[25,27] From ^{15}N CPMAS measurements ran in parallel, estimated Δ_{CSA} values are small here (close

TABLE 2: ^{81}Br NMR Parameters of *n*-Alkyltrimethylammonium Bromide Salts $C_xH_{2x+1}(CH_3)_3N^+Br^-$ [a]

	MAS (kHz)	δ_{iso} [b] (ppm)	C_Q (MHz)	η_Q	Δ_{CSA} (ppm)	η_{CSA}	ϕ (deg)	χ (deg)	ψ (deg)
TMAB ($x = 1$)	14	46.1	6.03	0.026	−22	0.2	0	1	10
	7	45.6	6.03	0.025	−18	0.8	17	12	7
	0	45.4	6.03	0.013	−18	0.2	10	3	10
average		45.7	6.03	0.02					
standard deviation		0.3	0.002	<0.01					
DTAB ($x = 12$)	30	59	7.27	0.137					
	14	57	7.32	0.101	65	0.7	36	68	81
	7	59	7.53	0.099	58	1.0	49	70	45
	0	59	7.44	0.120	70	0.3	33	66	25
average		58.6	7.39	0.11					
standard deviation		0.9	0.10	0.02					
TTAB ($x = 14$)	30	57	7.57	0.131					
	14	55.3	7.57	0.143	64	0.6	26	113	50
	7	57.2	7.94	0.200	66	0.4	33	116	40
	0	57.5	7.89	0.169	63	0.4	20	115	51
average		56.7	7.74	0.16					
standard deviation		0.8	0.17	0.03					
HTAB ($x = 16$)	30	56	8.01	0.187					
	14	55	8.03	0.191	64	0.3	0	117	52
	7	56	8.07	0.194	66	0.4	34	116	39
	0	57	8.00	0.137	54	0.7	36	115	85
average		55.9	8.03	0.18					
standard deviation		0.8	0.03	0.02					
OTAB ($x = 18$)	30	55	7.99	0.185					
	14	53.4	8.04	0.185	62	0.6	23	116	60
	7	54.2	8.14	0.193	62	0.5	30	117	44
	0	54.3	8.13	0.186	52	0.7	34	114	85
average		54.2	8.08	0.19					
standard deviation		0.5	0.07	<0.01					

[a] Standard deviation reports the actual distribution of measured parameters for the different acquisition conditions, which is larger than the mathematical errors computed from the covariance matrices or the Monte Carlo approach. [b] Relative to KBr span at 2−5 kHz.

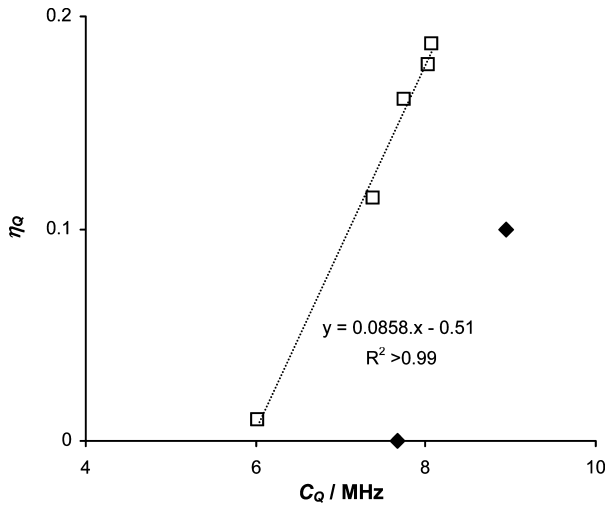

Figure 7. Variations of ^{81}Br η_Q as a function of C_Q: (□) data from spectrum modeling, (♦) data from theoretical calculations. The dashed line shows an empirical correlation between C_Q and η_Q parameters.

to 0 ppm for TMAB, and near −11 ppm for HTAB). In addition, we have tried to model the full spectra by taking the CSA interaction into account as well as the Euler angles (ϕ, χ, ψ) which describe the relative orientation of the QUAD and CSA interaction tensors.[25,38] After several trials with different modeling conditions, and even recording ^{14}N spectra at higher magnetic field, we were unable to reach a satisfying and an improved modeling of our experimental spectra. Therefore, the CSA interaction is not the main explanation here for nonsymmetrical SSB which has already been observed by other authors and ascribed to experimental artifacts on broad spectra. Despite these difficulties, we consider that the isotropic chemical shifts and the quadrupolar interaction parameters are accurately measured. This is further supported by the consistency with the values of C_Q and η_Q previously reported for TMAB and HTAB analyzed at smaller principal fields (Table 1).

From the ^{14}N NMR parameters presented in Table 1 and Figure 3, we observe that TMAB has ^{14}N NMR parameters noticeably different from the other salts. For $C_xH_{2x+1}(CH_3)_3N^+Br^-$ ($12 \leq x \leq 18$), δ_{iso} values (relative to NH_4Cl spinning at 4 kHz) are constant within error bars and equal to 13.0 ppm (Figure 3a),[76] while the quadrupolar interaction parameters vary significantly. We observe a small decrease of C_Q (from 107.2 to 96.9 kHz) and an evolution of η_Q (from 0.90 to 0.84) when increasing the chain length x (Figure 3b and c).

III.1.2. ^{81}Br. Solid state ^{81}Br MAS spectra of the same *n*-alkyltrimethylammonium bromide salts have been recorded at a high magnetic field $B_0 = 17.6$ T ($\nu_0 \equiv 202.60$ MHz) in order to decrease the effect of the quadrupolar interaction. Spectra obtained at the MAS frequency $\nu_{MAS} = 14$ kHz are presented in Figure 4. The spectrum of TMAB ($x = 1$) differs strongly from that of the other bromide salts ($12 \leq x \leq 18$) at this and other ν_{MAS} values. The effects of varying ν_{MAS} are shown for TMAB ($x = 1$) and for HTAB ($x = 16$) in Figures 5 and 6, respectively.[77] At fast MAS (14 kHz for TMAB in Figure 5a, 30 kHz for HTAB in Figure 6a), SSBs are strongly reduced and the isotropic line has the characteristic shape of a quadrupolar second-order broadened peak at infinite spinning rate. When ν_{MAS} decreases, spectra with more complicated line shapes are acquired due to the interplay of second-order quadrupolar and CSA interactions.

Obviously, modeling of these spectra is not a trivial task. However, it may allow the extraction of the isotropic chemical shift δ_{iso}, the C_Q and η_Q parameters of the

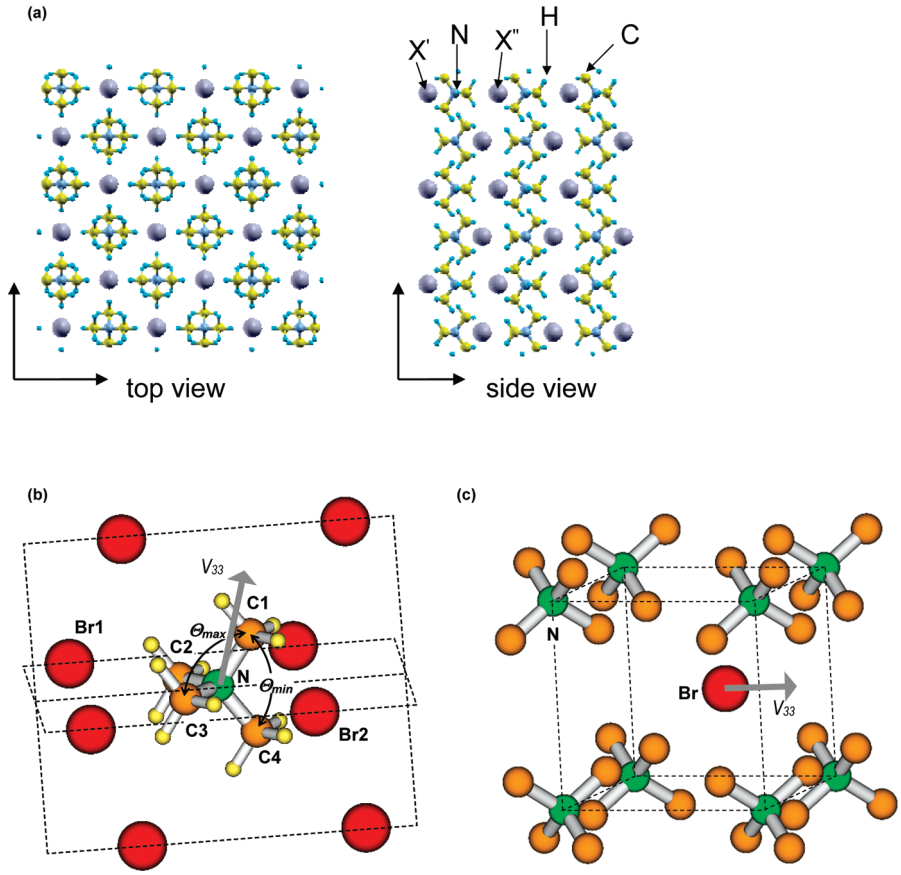

Figure 8. TMAX structures: (a) Schematic presentation of the TMAX structure. (b) Schematic presentation of the local site geometry of $(CH_3)_4N^+$ cations from the optimized structure of TMAB. This is the type of $[(CH_3)_4N \cdot X_8]^{7-}$ cluster (X ≡ Cl, Br, and I) used for the NMR property calculations within the cluster approach. (c) Schematic representation of the halide anion environment (here from optimized TMAB structure). Hydrogen atoms are omitted for the sake of clarity.

TABLE 3: B3LYP-DFT Optimized Geometrical Parameters, Mulliken Charges (q), for TMAX (X = Cl, Br, I) Structures Obtained within the Periodic Approach (Crystal03)[a]

crystal	NH_4Cl	TMACl	TMABr	TMAI
		Structural Data		
r(N−C)		1.503	1.502	1.502
r(C−H′)	1.033	1.090	1.089	1.090
r(C−H″)	1.033	1.091	1.091	1.091
r(N−X2)	3.31	4.28	4.40	4.50
r(N−X1)	3.31	5.30	5.13	5.25
θ_{min} (deg)	109.47	108.9	108.7	108.2
θ_{max} (deg)	109.47	109.8	109.9	110.1
$[\theta_{Td} - \theta_{min}]$ (deg)	0.0	0.6	0.8	1.3
$[\theta_{max} - \theta_{min}]$ (deg)	0.0	0.9	1.2	1.9
		Mulliken Charges		
qX	−0.86	−0.88	−0.91	−0.93
qN	−0.57	−0.36	−0.37	−0.37
qC		−0.21	−0.19	−0.18
qH	0.36	0.18	0.17	0.16

[a] The distances, r, are in Å, the angles are in degrees, and the atomic notations are shown in Figure 8.

quadrupolar interaction, the Δ_{CSA} and η_{CSA} parameters of the CSA interaction, as well as the Euler angles (ϕ, χ, ψ), data which are not yet accessible for $^{79/81}$Br containing compounds.[42] We were able to simulate the entire series of spectra by estimating a first set of C_Q and η_Q values from the fast MAS spectra and subsequently using these values as starting points for the modeling of the other spectra. All of the proposed models and their difference spectra are presented in Figures 5 and 6 or as Supporting Information. The differences between all ^{81}Br spectra and their mathematical models are small. On the static ^{81}Br spectrum of TMAB, a notch that could not be modeled is observed in the powder line shape (Figure 5c). It corresponds to an orientation of the V_{33} tensor element at the magic angle 54.7° with respect to the principal magnetic field axes, and it remains when ^{1}H decoupling is off (not shown). A similar line shape's feature was noticed on the static ^{17}O{^{1}H} CP spectrum of polycrystalline $Mg(OH)_2$.[78,79] It was explained by variations in the effectiveness of the CP due to specific relationships between the orientations of V_{33} and the dipolar coupling ^{1}H−^{17}O. This explanation does not work here, and we are still trying to find a satisfactory answer, remarking that this feature is unique to the case of TMAB and cannot simply be due to inefficient excitation of part of the crystallite orientation, as it would be present on all spectra. Nevertheless, the parameters found by modeling the static spectrum of TMAB are very close to those obtained from MAS spectra. The estimated parameters (QUAD, CSA, Euler angles) are listed in Table 2. For each bromide salt, we observe that the values of ^{81}Br NMR parameters estimated for the different ν_{MAS} are very close. This is particularly true for δ_{iso} (standard deviations represent less than 5%), and also for C_Q and η_Q, which is a strong indication about the consistency of the modeling procedures. In the following, we consider the average values for δ_{iso}, C_Q, and η_Q.

Results of ^{81}Br experiments and modeling are reported in Table 2 and Figure 3. As in the case of ^{14}N, the chemical shift of TMAB (45.7 ppm) is significantly different from that of the

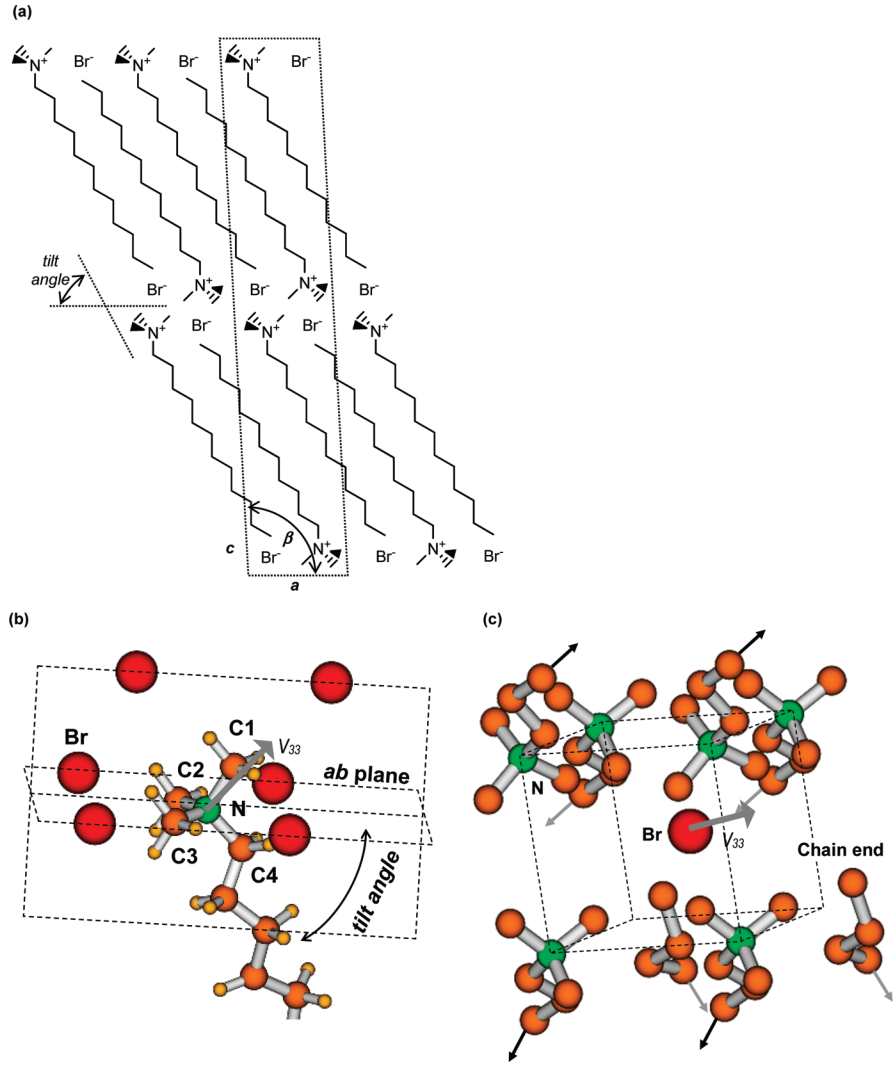

Figure 9. Long chain *n*-alkyltrimethylammonium bromide salt $C_xH_{2x+1}(CH_3)_3N^+Br^-$ structures. (a) Schematic presentation of the bilayered structure. (b) Schematic presentation of the local site geometry of the polar head groups $-CH_2(CH_3)_3N^+$. (c) Schematic representation of the Br^- environment. Hydrogen atoms are omitted for the sake of clarity.

other salts for which we observe in Figure 3a a decrease of δ_{iso} from 58.6 to 54.2 ppm as a function of x for the surfactant crystals ($12 \leq x \leq 18$). For the quadrupolar interaction parameters, we observe an increase of C_Q and η_Q as a function of x (Figure 3b and c). Both parameters show indeed an interesting linear correlation (Figure 7). The other parameters' values (CSA, Euler angles) may also follow some general trends as a function x, but they are less accurate and therefore less informative.

III.2. X-ray Crystal Structures and Theoretical Calculations. ***III.2.1. TMAX Salts.*** In order to correlate crystal structures and NMR interactions, we first considered salts of the small TMA^+ cations for which experimental data are available. Optimized structural parameters and quadrupolar interaction parameters for three TMAX (X ≡ Cl, Br, or I) salts, computed at the DFT level, were used to give more insight into the relationship between the chemical nature of halide ions, structural parameters, and C_Q and η_Q values. At low to ambient temperature ($T < 300$ K), the TMAX crystals are known to have the CsCl-type crystal arrangement with 8-fold coordination organized in the *P*4/*nmm* symmetry space group, as shown in Figure 8a.[57] Optimized geometrical parameters of TMAX and NH_4Cl bulk structures are collected in Table 3. Deviations of the TMAX optimized structures from the experimental ones are less than 4.5%. The computational results reveal high similarity of the structural parameters in the three TMAX salts. In the case of the reference system, NH_4Cl, the r(N−H) distance obtained from our geometry optimization agrees very well with the previous periodic *ab initio* calculations.[80] The atomic charges from the Mulliken population analysis for the three TMAX compounds, listed in Table 3, reveal charges of the halide and nitrogen atoms equal to −0.88 to −0.93 and −0.36 to −0.37 e^-, respectively. Carbon and hydrogen atomic charges also do not vary significantly with the halide anions.

The resulting site geometry of the TMA^+ cations is presented in Figure 8b. Here, the optimized structure of TMAB has been chosen as an example. The local symmetry of TMA^+ is D_{2d}. In addition, we observe that the Br^- counteranions, the two C2 and C3 atoms, and the N atoms are located in the same plane. A second plane containing C1, C4, and N atoms is perpendicular to the first one. The shorter r(N−Br2) distance corresponds to r(N−X2) in Table 3 for other halide anions. The value of r(N−X2) increases slightly with the halide atomic number, whereas no similar correlation is obtained for the variation of the larger r(N−X1) distance (Table 3). The N−C and C−H bond lengths are also very alike, thus leading to a conclusion that the bond lengths in the tetramethylammonium cation (TMA^+) are not affected by the nature of the X anions.

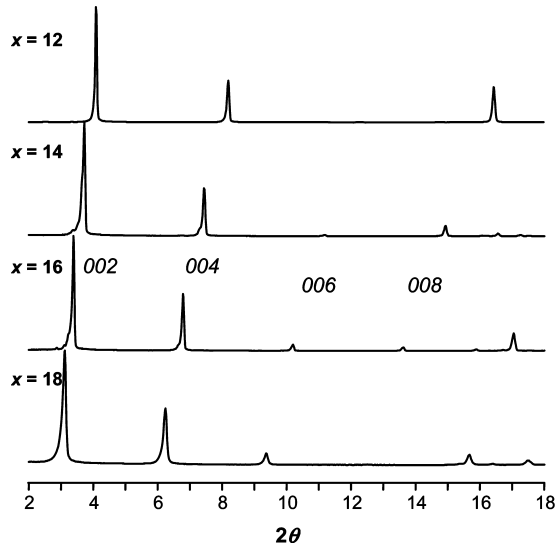

Estimated unit cell parameter c and deviations to ideal bilayers $(1 - c / c_{max})$:

x	12	14	16	18
c (Å) for $P2_1/c$	43.10	47.42	52.01	56.59
$(1 - c / c_{max})$ [a]	0.039	0.050	0.054	0.057
$(1 - c / c_{max})$ [b]	0.128	0.129	0.125	0.125

a: c_{max} comes from l_{max} estimated using Tanford values (see Experimental).
b: c_{max} comes from l_{max} estimated using crude geometrical optimizations (see Experimental).

Figure 10. Small-angle X-ray diffractograms of long chain *n*-alkyltrimethylammonium bromide salts $C_xH_{2x+1}(CH_3)_3N^+Br^-$. Unit cell parameters c are determined from peak position and used to evaluate the deviation from ideal bilayers $(1 - c/c_{max})$ by different approaches (see the Experimental and Results sections).

TABLE 4: Crystal Structures of Long Chain *n*-Alkyltrimethylammonium Bromide Salts $C_xH_{2x+1}(CH_3)_3N^+Br^-$

x:	12	14	14	16	16	16	16
reference:	82	81	84	81	83	polymorph III in ref 45	polymorph III optimized
space group	$P2_1/m$	$P2_1/c$	$P2_1/c$	$P2_1/c$	$P2_1/c$	$P2_1$	$P2_1$
a (Å)	5.64	5.65	5.63	5.64	5.64	5.63	5.63
b (Å)	7.26	7.29	7.24	7.27	7.26	7.25	7.25
c (Å)	21.06	47.46	47.39	52.08	52.07	26.01	25.94
β (deg)	86.85	91.23	91.17	93.81	93.78	93.78	93.78
tilt angle chain vs *ab* plane (deg)	67				65	64	
				Bond Angles			
C1−N−C4	106.6		111.5		106.3	106.5	113.0
C2−N−C4	111.2		106.4		111.0	102.5	106.9
C3−N−C4	111.2		111.7		112.5	123.3	109.8
average Ci−N−Cj (i,$j \leq 3$)	109.2		109.1		109.0	107.5	109.0
				N−C Distances			
average r(N−Ci) ($i \leq 3$)	1.50		1.50		1.50	1.49	1.51
r(N−C4)	1.51		1.51		1.50	1.45	1.51
				N−Br Distances			
short r(N−Br)	4.21		4.19		4.20	4.09	4.19
	4.21		4.21		4.22	4.29	4.25
	4.51		4.54		4.56	4.56	4.54
average	(4.31)		(4.31)		(4.33)	(4.32)	(4.33)
long r(N−Br)	5.05		5.04		5.05	4.99	5.00
	5.05		5.06		5.06	5.12	5.06
	5.18		5.16		5.17	5.15	5.13
average	(5.10)		(5.08)		(5.09)	(5.09)	(5.06)

[a] The distances, r, are in Å, the angles are in degrees, and the atomic notations are shown in Figure 8.

However, the size of the halide anion influences the bond TMA^+ angle. Two sets of bond angles exist: θ_{min} for ∠(C1−N−C4) and ∠(C2−N−C3) and θ_{max} for the four others. As presented in Table 3, we obtained a θ_{min} bond angle smaller than 109.47° in the perfect T_d structure (θ_{T_d}) and a θ_{max} bond angle larger than θ_{T_d}. In going from TMAC to TMAB to TMAI, a decrease of θ_{min} and an increase of θ_{max} are observed. As a result, the difference $(\theta_{T_d} - \theta_{min})$, which represents a deviation from T_d symmetry increases to 0.6° (TMAC), 0.8° (TMAB), and 1.3° (TMAI), respectively. The 8-fold coordination of halide anions in the TMAX salts is shown in Figure 8c (optimized structure of TMAB). The eight TMA^+ cations are located at the corners of a rectangular parallelepiped in a C_{4v} local symmetry arrangement around the X^- anions. The anions are closer to one side of the parallelepiped (the distance r(N−X2) = 4.4 Å for X ≡ Br). At the other side of the parallelepiped, r(N−X1) distances are greater (5.1 Å for X ≡ Br) but r(C−X) distances are smaller and methyl groups are pointing toward the X atom.

III.2.2. $C_xH_{2x+1}(CH_3)_3N^+Br^-$ Salts. The presently known crystal structures of *n*-alkyltrimethylammonium bromide salts $C_xH_{2x+1}(CH_3)_3N^+Br^-$ ($12 \leq x \leq 18$) all belong to the monoclinic space group $P2_1$.[45,81−84] The general model that can be proposed accounts for the layered structure of the *n*-alkyl chains built from sheets of alternating trimethylammonium head groups and bromide anions with distinct intersheet spaces occupying the *n*-alkyl chains pointing outward to the unoccupied void space (Figure 9a).

In order to gain more information on the bulk polycrystalline material which is normally used in the production of mesoporous materials and in households after dilution of the surfactants, we recorded the small-angle X-ray diffractograms of the powdered samples studied by NMR (Figure 10). Furthermore, the small-angle X-ray diffraction traces enable us to characterize the solid polycrystalline material used in the solid state NMR experiments, and to compare the results with those known from single crystal X-ray diffraction analysis. The observed diffraction traces were assigned to the (00*l*) planes of bilayer structures with a $P2_1/c$ space group, as found in most published structures (Table 4). Qualitatively, we observe that the relative intensities of the diffraction peaks are not the same for each polycrystalline sample investigated. Particularly, it was observed when the chain length increases the magnitude of the (006) peak increases but the (008) peak decreases (Figure 10), an indication of a variation in the crystal packing. In addition, the longest cell parameter *c* of the unit cell was estimated from the positions of the 00*l* diffraction peaks. The values obtained are very close to most of the polymorphs reported in the literature (Table 4). As expected, there is a gradual increase of *c* from DTAB to OTAB.

Assuming an ideal crystalline unit cell built from bilayers and fully extended *n*-alkyl chains perpendicular to these bilayers, one can crudely estimate a maximum value c_{max} for the unit cell parameter *c* by adding two diameters of Br^- anions (ionic radius of 1.96 Å) and twice the maximum length l_{max} of the $C_xH_{2x+1}(CH_3)_3N^+$ cations. Accordingly, it is possible to estimate the deviation from this ideal unit cell ($1 - c/c_{max}$) as well as the tilt angles between the chains and the bilayers as a function of *x* the number of carbons in the *n*-alkyl chains. The results depend on the method used for the estimation of l_{max} (see Experimental Methods and Figure 10). However, it appears that ($1 - c/c_{max}$) deviations are low and that their variations as a function of *x* are even smaller (less than 5%). The estimated tilt angles are in the 60−75° range, in agreement with previous crystallographic data (see below). Therefore, from these estimations, the polycrystalline samples analyzed by NMR have very similar structures. We try to gain more information from previously published crystal structures, whose unit cell parameters may fit with our small-angle XRD data. These structures correspond to DTAB, TTAB, and HTAB (Table 4), but results might be extrapolated to OTAB.

The experimental atomic positions in the $P2_1$ unit cell of HTAB polymorph III[45] (Supporting Information) were optimized using the same theoretical approach as that used for the TMAX structures (see Experimental Methods). We note that the unit cell parameters of polymorph III[45] are in accordance with our XRD results (Table 4 and Figure 10) and are also close to previously published data.[81,83] The HTAB optimized geometrical parameters are reported in Table 4, together with experimental data from this and previous studies. The differences between experimental and computed interatomic distances and bond angles in the trimethylammonium cation group of HTAB are more significant when compared with the TMA^+ cation in TMAX salts. The geometry optimization results yielded smaller a difference between the six values of ∠C−N−C angles in the tetrahedron structure around N and equivalent N−C bond lengths between the N and the C atoms of the three methyl groups, when compared with the crystallographic data. The computed six *r*(N−Br) distances may be grouped into two averaged distances: a short one of 4.33 Å and a long one of 5.06 Å. It is noteworthy that these two values are very similar to the two *r*(N−Br) distances obtained for the optimized TMAB structure. Mulliken atomic charges of −0.92 (Br) and −0.41 (N) atoms also very much resemble the ones for the Br and N charges in the TMAB. Carbon atomic charges in the long chain *n*-alkyltrimethylammonium bromide salt are −0.15, −0.15, −0.13, and −0.09 for C1, C2, C3, and C4 atoms, respectively.

For all of the structures presented in Table 4 which correspond to the polycrystalline samples studied by NMR (see XRD data above), the sheets are parallel to the *ab* plane. Also, the unit cell parameters are almost identical for the known structures: $a = 5.64 \pm 0.01$ Å and $b = 7.26 \pm 0.03$ Å. In addition, there are two planes parallel to *ab* that contain N, C2, C3, and almost Br atoms (Figure 9b), Br being slightly out of plane (about 0.29 Å for HTAB[83]). In these planes, N−C bonds follow roughly the diagonals of an *ab* rectangle. From these observations, it appears that the arrangement of the ionic groups gives rise to a preferential rectangular network (sheets) which can be considered as identical for all crystals, and that might constrain the *n*-alkyl chain packing.

The *n*-alkyl chains are almost in a fully extended conformation.[45,83,84] For the carbon atoms, some positional disorder[82] and vibrational motions in planes normal to the chain axes[45] have been noticed. This positional disorder is increased for the last C atom of the chain, the methyl groups, as observed for all crystals. Also, the dihedral angles slightly deviate from 180° at the proximity of the polar headgroup.[83,84] Tilt angles between the *n*-alkyl chains and the *ab* planes are close and between 64−65° for HTAB[45,83] and 67° for DTAB.[82] Again, *n*-alkyl chain packing seems not to be very different from one structure to the other. Morevover, for all of the reasons developed above, the studied crystal structures appear to be very similar. The difference observed in XRD peak intensities (006 vs 008 in Figure 10) might depend on the relative orientation of the sheets between themselves and are more likely related to differences in the values of the angle β (Figure 9a, Table 4).

The local site geometry of the polar head groups $-CH_2(CH_3)_3N^+$ is schematically presented in Figure 9b. The bromide ions are arranged in a sort of plane trigonal bipyramidal geometry with respect to the ammonium group. As already mentioned, two N−C bonds (C2, C3) are in one plane and parallel to the *ab* plane. The two other N−C bonds (C1, C4) point out of this plane but belong to a second plane roughly perpendicular to the first one. A picture emerged which is similar to the site geometry of the TMA^+ cations (Figure 8b). The distribution of N−C bond distances is akin for all of the crystals, but C−N−C bond angles slightly differ from one crystal structure to another (Table 4). Main differences are observed for C−N−C bond angles involving C4 atoms of the *n*-alkyl chain, whereas angles between C atoms of methyl groups are closer together. The general site geometry of the polar groups is common to the known crystal structures of the salts studied, and the differences probably originate from the changes in the bond angles.

In Figure 9c, the local site geometry of the bromide anions is schematically presented. There are no close contacts between anions. The Br atoms are virtually inside a rectangular parallelepiped, as seen for the TMAX salts, but the corners contain now six ammonium groups and two pending groups of *n*-alkyl chain ends instead of eight tetramethylammonium cations. Thus, the charges are less symmetrically distributed. Like in TMAX salts, the Br atoms are closer to one side of the parallelepiped. The shorter *r*(N−Br) distances are in the 4.1−4.6 Å range (Table 4). And the averaged *r*(N−Br) distances take a value of 4.3 Å for all known structures, which is very close to the smallest *r*(N−Br2) distance found in TMAB (Table 3). The longer *r*(N−Br) distances are in the 5.0−5.2 Å range. And the averaged

TABLE 5: Calculated ^{14}N and ^{81}Br Quadrupolar Parameters

crystal	NH_4Cl	TMAC	TMAB	TMAI	HTAB
		^{14}N Parameters			
experimental					
C_Q at $T = 293$ K (kHz)		17[a], 18[d]	25−27[a−d]	31−32[a,d,e]	98[a,b]
C_Q at $T \sim 223$ K (kHz)				35[a]	95[a]
C_Q at $T \sim 190$ K (kHz)		17[a]		36[a]	
C_Q at $T = 155$ K (kHz)		40[a]			
η_Q at $T = 293$ K		0[a]	0−0.04[a−c]	0[a,e]	0.84[b]
calculated-periodic					
C_Q (kHz)	0	37	46	66	120
η_Q	0	0	0	<0.01	0.81
calculated-cluster $[N(CH_3)_4X_8]^{7-}$					
C_Q (kHz)	0	38	51	79	
η_Q	0	0	0	<0.01	
C_Q (293 K)/C_Q (calculated periodic)		0.46	0.57	0.48	0.82
		^{81}Br Parameters			
experimental					
C_Q (MHz)			6.03[b]		8.03[b]
η_Q			0.02[b]		0.18[b]
calculated-periodic					
C_Q (MHz)			7.66		8.95
η_Q			0.00		0.10
C_Q (293 K)/C_Q (calculated periodic)			0.79		0.90

[a] Reference 41. [b] This work. [c] Reference 86. [d] Reference 40. [e] Reference 38.

r(N−Br) distances take a value of 5.1 Å, close again to the second r(N−Br1) distance in TMAB (Table 3). Methyl groups bound to N have also a similar arrangement to that in TMAB and a similar set of r(C−Br) distances.

III.3. Calculated NMR Parameters. Table 5 lists the ^{14}N C_Q values of TMAX salts computed using DFT/B3LYP periodic and cluster calculation approaches. Cluster calculations were carried out for $[N(CH_3)_4X_8]^{7-}$ clusters cut from the optimized bulk TMAX structures (Figure 8b). The C_Q values from the periodic and $[N(CH_3)_4X_8]^{7-}$ cluster calculations agree well within 17%. Good agreement between periodic and cluster approaches was also concluded for the ^{23}Na C_Q calculations in a series of crystalline compounds.[85]

The tendency found for ^{14}N C_Q values is in agreement with our and other experimental works;[38,40,41,86] namely, the trend C_Q(TMAC) < C_Q(TMAB) < C_Q(TMAI) is obeyed. To our knowledge, there were no previous calculations for those compounds to compare with. The C_Q value from ^{14}N NMR measurements at $T = 155$ K in the case of TMAC[41] is in perfect agreement with the B3LYP C_Q value, whereas the ^{14}N C_Q value at $T = 293$ K is more than 2 times smaller (Table 5). The experimental ^{14}N C_Q value at $T = 293$ K for the TMAB is also approximately 2 times smaller than the computed value. Possible origins of these discrepancies will be rationalized below (see the Discussion). However, the agreement between our calculated and experimental results for the ^{81}Br quadrupolar parameters of TMAB is rather good (Table 5).

Analysis of the TMAX electron structures showed no covalent interaction between the tetramethylammonium and halide ions. The same conclusion was reached for NH_4Cl in an earlier *ab initio* study.[80] From the nearly cubic arrangement of the eight anions around the cation, one expects that the electric field created by the halides will not cause changes in the electric field gradient (EFG) at the nitrogen nucleus. Therefore, to examine the role of the halide anions on the NMR quadrupolar interaction, we recalculated the QUAD parameters only for the TMA^+ ions by fixing the $[N(CH_3)_4]^+$ geometries in the optimized TMAX cells (periodic B3LYP structures). The same type of computations was performed for the TMA^+ cations embedded in eight point charges at the crystal X^- positions of whatever charges. These sets of calculations yielded very similar NMR QUAD parameters agreeing within a margin of 10−15% with those in the presence of X^- in $[N(CH_3)_4X_8]^{7-}$ clusters or in the crystal lattices, demonstrating that the presence of anions in the TMAX crystals influences only the TMA^+ geometrical structure. Particularly, TMA^+ structural changes reflect the deviation from the perfect tetrahedron arrangement, giving rise to different ^{14}N C_Q values by changing the halide anions (Cl, Br, and I) in the salt lattices. These results are discussed in detail below (see the Discussion).

The ^{14}N C_Q is significantly higher in HTAB when compared with TMAB. The B3LYP C_Q value agrees well with the experimental one obtained at $T = 293$ K (Table 5). Replacement of one methyl group by one *n*-alkyl chain deforms notably the tetrahedral symmetry around the nitrogen, as discussed above, and consequently, the V_{11} and V_{22} components of the EFG tensor differ by a factor of 9.5, resulting in an asymmetry parameter of $\eta_Q = 0.81$ in perfect agreement with our experimental η_Q. It is also interesting to note the relation between the three EFG components in HTAB and TMAX compounds at the nitrogen nucleus: in TMAX, we found $|V_{33}| = 2|V_{22}| = 2|V_{11}|$, whereas in HTAB we observed $|V_{33}| = 10.5|V_{22}| = 1.1|V_{11}|$.

The local environment around Br^- in HTAB also differs from that of Br^- in TMAB (Figures 8c and 9c), resulting in ^{81}Br C_Q and η_Q values in HTAB which are higher by 10−15% than those in TMAB (Table 5). The relation between the computed EFG components is the following: $|V_{33}| = 2|V_{22}| = 2|V_{11}|$ and $|V_{33}| = 2.3|V_{22}| = 1.8|V_{11}|$ in TMAB and HTAB, respectively.

The orientations of V_{33} in the principal axis system are also determined for the TMAB and HTAB salts and are shown in Figures 8b and c and 9b and c. The V_{33}(^{14}N) at nitrogen in TMAB forms an angle of 20° with the N−C1 bond (Figure 8b). Its orientation is not parallel to one of the C_3 or C_2 symmetry axes if the local TMA^+ site structure is considered. In HTAB, V_{33}(^{14}N) points toward a direction close to the N−C1 bond with a V_{33}−N−C1 angle of 7.6°. The V_{33}(^{81}Br) at the Br site in HTAB (Figure 9c) and TMAB (Figure 8c) are oriented

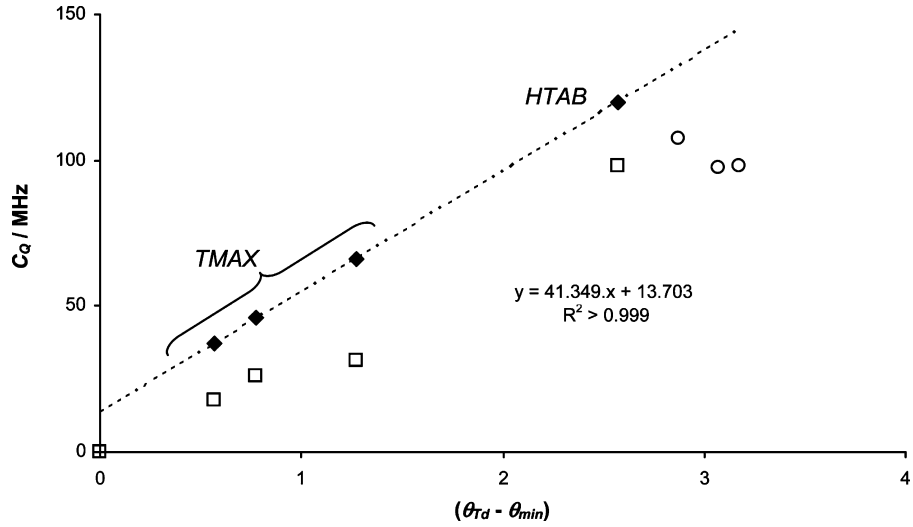

Figure 11. Variations of the ^{14}N quadrupole coupling constant C_Q as a function of the angle difference ($\theta_{T_d} - \theta_{\min}$) for (♦) calculated C_Q and optimized structures (TMAX, HTAB), (□) experimental C_Q and optimized structures (TMAX, HTAB), and (○) experimental C_Q and nonoptimized structures (DTAB, TTAB, HTAB). The dashed line shows the empirical correlation between calculated C_Q and ($\theta_{T_d} - \theta_{\min}$).

toward the closest sides of the parallelepiped rectangles formed by the neighboring organic groups.

Due to the lower symmetry of HTA^+ and Br^- local structures in HTAB, cluster calculations for those two sites need to include appropriate embedding with point charges in order to reproduce the crystal long-range electrostatic interactions, which is a demanding task. On the contrary, the long-range electrostatics in these highly ionic crystals is well reproduced when using the periodic approach. For the present study, however, we were more concerned about computing ^{14}N and ^{81}Br quadrupolar parameters of the optimized HTAB using analytical geometry optimization in the periodic approach (see Experimental Methods), and therefore, cluster calculations were not performed.

IV. Discussion

The experimental values found for the ^{14}N NMR parameters compare well with previous published data on salts of TMAB and HTAB, or other tetraalkylammonium halide salts.[38−41,86] In addition, no ^{81}Br NMR data are available in the literature for this family of compounds. For a better understanding of the relationship between structure and NMR parameters, a brief discussion of the obtained results will be offered.

IV.1. ^{14}N NMR Parameters. The differences in ^{14}N quadrupolar coupling (QUAD) interaction parameters may be reconciled by the changes in the molecular structures of the *n*-alkyltrimethylammonium cations. Replacing a methyl group with a long *n*-alkyl chain, the local symmetry of the quaternary nitrogen changes from near T_d to near C_{3v}. As a result, the ^{14}N C_Q values increased from 26.5 to 95−107 kHz. The increase in C_Q is more significant when passing to a near C_{2v} symmetry at the N atom, e.g., in DDAB (didodecyldimethylammonium bromide) as reported earlier from static ^{14}N spectra (C_Q = 190 kHz)[41] and as confirmed by us in parallel MAS experiments (C_Q around 150−200 kHz). The differences in molecular structure may also explain the difference in $\delta_{iso}(^{14}N)$ of c.a. 3.8 ppm between TMAB and the series of *n*-alkyltrimethylammonium bromide $C_xH_{2x+1}(CH_3)_3N^+Br^-$ ($12 \le x \le 18$) (Table 1). However, this simple approach does not account for the observed differences in C_Q and η_Q (Tables 1 and 3) when varying the length of the alkyl chains ($12 \le x \le 18$) or changing the nature of the counteranion (Cl^- or I^- instead of Br^-).

IV.1.1. Small TMA$^+$ Cations. An interesting starting point for studying the relationships between NMR parameters and chemical structures using theoretical calculations is the case of the small TMA^+ cations in TMAX salts. The optimized structure (T = 0 K) of the single TMA^+ molecule is highly symmetric, and the resulting C_Q is almost zero. C_Q values between 17 and 32 kHz have been measured at T = 293 K in real TMAX crystals. The calculated values (T = 0 K) are always higher (Table 3). These differences in C_Q can arise from differences in mobility of the cations. Internal mobilities involving the TMA^+ cations inside TMAX salts have been reported in the past.[87−92] Several types of movements occur: rotation of the methyl groups around the C−N C_3 axes, rotation of TMA^+ cations by site jumps around the C−N C_3 and C_2 axes, and isotropic tumbling of TMA^+ cations. From ^{1}H and ^{2}H NMR data,[89,91,92] it has been shown that the first type (methyl rotation) starts at low temperature (T around 150−170 K) and it is not expected to strongly modify the EFG at the N site. The other types of movement start at slightly higher temperatures and can be combined together and possibly modify the ^{14}N quadrupolar coupling interaction. In addition, it has already been observed that the ^{14}N C_Q values decrease from 40 kHz (T = 155 K) to 17 kHz (T = 293 K) for the TMA^+Cl^- salt (TMAC).[41]

Our theoretical calculations yield, for TMAC at T = 0 K, C_Q values between 30 and 38 kHz in agreement with the experimental C_Q value found at T = 155 K (Table 3). The ratio between the experimental C_Q (at T = 293 K) and the calculated C_Q is approximately 0.5. The obtained results for TMAC may be extrapolated to other tetramethylammonium halide salts, e.g., TMAB and TMAI. The calculated (T = 0 K) and experimental values (T = 293 K) always follow the order C_Q(TMAC) < C_Q(TMAB) < C_Q(TMAI) (Table 5). This result is consistent with the order of the size of the ionic radii of the halide as counteranions. In addition, the ratio between the experimental and calculated C_Q is again about 0.5, indicating a close similarity of the mobility of TMA^+ cations in these salts as expected. Furthermore, we have shown that V_{33}, the more intense EFG tensor element, is not parallel to any of the C_3 or C_2 symmetry axes. Thus, rotations of TMA^+ around C_3 or C_2 axes would indeed decrease C_Q.[93] Therefore, the mobility of the tetramethylammonium cations affects the ^{14}N C_Q experimental values but there is still a significant effect of the nature of the counteranions.

The chemical nature of the counteranion has only an indirect effect on the final C_Q. Replacing halide anions by point charges of different value in the cluster calculation approach has no

significant effect on the EFG tensor (see Results). Therefore, the nature of the counteranion mainly influences the crystal packing and hence the symmetry of the methyl groups around the nitrogen as observed form the similarity between periodic and cluster methods. By inspecting distances and dihedral angles of the structures used for the calculations, we found that the major changes are observed for the C−N−C angles, θ_{min}, and θ_{max} (Table 3). The deviation from T_d symmetry exemplified by the bond angle difference ($\theta_{T_d} - \theta_{min}$) increases by increasing the size of the halide counteranions. In addition, in Figure 11, one notes a gradual correlation between increasing C_Q values and an increase in the difference ($\theta_{T_d} - \theta_{min}$). Consequently, the deviation from a pure T_d symmetry causes the differences in C_Q values for the TMAX series. One could thus speculate that the mobility of the TMA^+ cations (*vide supra*) would also reduce this ($\theta_{T_d} - \theta_{min}$) bond angle difference in the TMAX at room temperature. In order to prove this assumption, calculations involving molecular dynamics methodologies at finite temperatures are in progress. Finally, since the local symmetry of the TMA^+ cations is D_{2d}, the asymmetry parameter η_Q still remains close to 0.

IV.1.2. Long Chain n-Alkyltrimethylammonium Bromide Salts. Site jumps are probably excluded for the *n*-alkyltrimethylammonium cations with long *n*-alkyl chains, although some other internal mobility may occur. By taking the experimental values into account, ^{14}N C_Q values reported here for HTAB and in a previous report but at different temperatures[41] are close (Table 1). C_Q values even increase slightly with temperature for various surfactant salts,[41] suggesting the presence of small variations in the crystal structure. In addition, the C_Q values reported for HTA^+ cations subjected to motions in liquid crystal phases or mesophases are found to always be lower.[21,22,94] Moreover, from theoretical calculations, C_Q was estimated to 120 kHz for HTAB, a value which is close to the experimental one (∼20% difference). Taking all of these reasons into account, a significant effect of the mobility in the ^{14}N quadrupolar interaction parameters of long chain *n*-alkyltrimethylammonium bromide salts can be ignored. If we also consider the asymmetry parameter η_Q, the agreement is excellent between experimental values obtained at $T = 293$ K (0.84) and calculated values at $T = 0$ K (0.81).

IV.1.3. TMAB−HTAB Comparison. Experimental and calculated ^{14}N quadrupolar interaction parameters are different for TMAB and HTAB. From optimized crystal structures, we observe practically no differences in the four shortest N−C distances and slightly different Mulliken charges. In particular, the charge of C4 in HTAB is much closer to zero than that in TMAB. Furthermore, significant changes are noticed for the C−N−C angles involving the C4 atom. The replacement of a methyl group by an *n*-alkyl chain at this C4 position is responsible for these changes. The *n*-alkyl chain is closely packed to neighboring chains and this imposes a specific distribution of angles around the nitrogen. If we consider θ_{min} as being the lowest C−N−C angle of the optimized HTAB structure (106.5°), the correlation found for TMAX between calculated or experimental C_Q values and the angle difference ($\theta_{T_d} - \theta_{min}$) remains valid (Figure 11). There is even an empirical linear correlation for the calculated C_Q values.[95] All of these observations suggest that the spatial distribution of CH_x groups around the N atoms, defined here by the C−N−C angle distribution, strongly influences the intensity of the ^{14}N quadrupolar coupling constant C_Q.

The spatial distribution of bromide anions also plays a role, and we expect to observe strong differences in quadrupolar interaction parameters arising from the absence of two bromide anions at the vicinity of the nitrogen in the case of long chain *n*-alkyltrimethylammonium bromide salts (Figure 8b vs Figure 9b). From theoretical calculations, the orientation of V_{33} is very similar and close to the N−C1 bond. In addition, the intensity of V_{33} might be mainly affected by the C−N−C angles as deducted from C_Q variations (*vide supra*). However, major changes are noticed for the values of V_{11} and V_{22} terms, contributing to contrast the η_Q values. It should be mentioned that the scalar value V_{22} is very close to that of V_{11} for the HTAB contrary to the TMAX case (see Results).

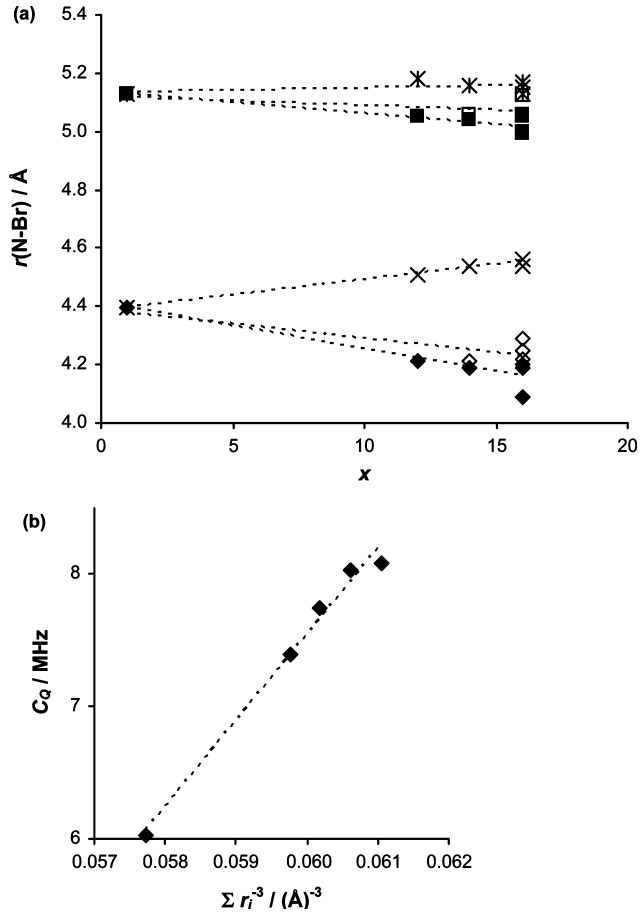

Figure 12. (a) Variations of the r(N−Br) distances as a function of the alkyl chain length x (with all known or optimized r(N−Br) values). The dashed lines correspond to empirical linear fits from which r(N−Br) are recalculated into the r_i values. (b) Variations of the ^{81}Br quadrupole coupling constant C_Q as a function of the sum $\sum r_i^{-3}$, where r_i are the recalculated values for the r(N−Br) distances as in part a.

IV.1.4. Effect of Chain Length. Experimental ^{14}N quadrupolar interaction parameters are slightly different for each of the long chain *n*-alkyltrimethyl ammonium bromide salts $C_xH_{2x+1}(CH_3)_3N^+Br^-$, but the differences remain low in particular for $14 \leq x \leq 18$. From the crystallographic data, no clear differences in the structures are noticed except for the variations in C−N−C angles. We anticipate that these variations are related to the differences observed in quadrupolar interaction parameters, but atomic positions and calculations are not yet precise enough to account for this. Work is in progress to elucidate this including other *n*-alkyltrimethylammonium halide salts in order to asses the effect of structure or local symmetry.

IV.2. ^{81}Br NMR Parameters. Bromide anions are not chemically bound to other atoms in the crystals studied and have no close contact with other anions. Therefore, their ^{81}Br NMR

interactions mostly depend on the spatial distributions of the cations around the anions.

As noticed from their crystal structures, Br^- anions are not located at the center of the rectangular parallelepipeds defined by their closest chemical groups. They are not in a fully symmetric position, and ^{81}Br quadrupolar coupling interaction parameters are nonzero. However, the environment of Br^- anions differs in TMAB and in long chain *n*-alkyltrimethylammonium bromide crystals, e.g., HTAB (Figure 8c vs Figure 9c). Instead of eight TMA^+ cations, Br^- anions in HTAB are surrounded by six ammonium polar head groups and two pending methyl groups of the alkyl chain. This situation leads to different distributions of charges, and thus to different intensities and orientations for the terms of the EFG tensors. Indeed, two different sets of C_Q and η_Q quadrupolar interaction parameters are observed experimentally or theoretically. The agreement between experiment and theory here is about 80% for C_Q.

It is also important to note that the theoretical C_Q and η_Q values follow the same correlation as the experimental values (Figure 7). This correlation between experimental C_Q and η_Q values is linear ($R^2 > 0.99$) and is related to the chain length. The question is now how chain length variations may influence the spatial distribution of the cations or charges around the bromide anions. From the structural data (Table 4), the answer is not trivial. The variations in the *r*(N−Br) average distances are small and the precision of each distance might not be so high. However, the variations of known or optimized *r*(N−Br) distances as a function of the *n*-alkyl chain length show some features (Figure 12a). Interestingly, the smallest *r*(N−Br2) distance in TMAB splits into three sets of *r*(N−Br) values with variations which vary in a contradictory sense: two *r*(N−Br2) distances decrease with *x* and one *r*(N−Br2) distance increases with *x*. It is like bromide anions are getting closer to one side of the parallepiped as the chain length increases. This behavior may explain the gradual increase in C_Q by the shortening of the smallest *r*(N−Br) distances, and also in η_Q by the decrease in symmetry. In an electrostatic system, EFG is dependent on distances between charges and varies with r^{-3}. Using the empirical linear correlation fits between values of *r*(N−Br) and *x* depicted in Figure 12a, we are able to recalculate the *r*(N−Br) distances for each compound. Recalculated distances are denoted as r_i. We have tentatively plotted C_Q values as a function of the sum $\sum r_i^{-3}$ (Figure 12b). Although this analysis is reduced to simple terms, the observed gradual increase demonstrates the dependency of C_Q on the spatial distribution of the cations.

Chemical shift variations could also give some insight about the spatial distribution of the cations. Various authors have shown that δ_{iso} of halide anion is dependent on the anion−cation overlaps and thus related to anion−cation distances.[42,96] In addition, the effects are additive and may lead to strong variations. In the case of Br−Na pairs, it was empirically shown that a variation of 1 Å in *r*(Na−Br) distance would lead to a decrease of about 35 ppm in $\delta_{iso}(^{81}Br)$.[96] For the systems considered here, bromide anions are surrounded by six or eight organic cations, so the variations in δ_{iso} might be more complex. However, we noticed that δ_{iso} varies within 13 ppm for *r*(N−Br) distance variations within 0.8 Å (Figure 3a, Tables 2−4).

V. Conclusions

For a series of *n*-alkyltrimethylammonium bromide salts, the crystal structures were characterized by high quality ^{14}N and ^{81}Br MAS NMR spectra with the application of a high magnetic field in the case of ^{81}Br. The quadrupolar coupling interaction NMR parameters have been obtained by spectrum modeling, as well as the chemical shift anisotropy parameters and the Euler angles for ^{81}Br.

The crystal structures were found to be quite similar as deducted from X-ray diffractograms, NMR, and theoretical calculations. Conclusive evidence of the mobility of the small cations for TMAX salts and on the C−N−C angular deviation from T_d symmetry has been given through the ^{14}N parameters. Furthermore, the nature of the counteranion has an indirect effect on the ^{14}N NMR quadrupolar coupling interaction parameters by affecting the crystal structure and the symmetry of charges.

In the case of the long chain *n*-alkyltrimethylammonium bromide salts, theoretical calculations of both ^{14}N and ^{81}Br NMR quadrupolar coupling interaction parameters allowed us to study the relationships between crystal structures and NMR parameters in more detail. It appeared that the arrangement of the ionic groups gives rise to a preferential rectangular network (sheets) almost identical for all crystals, which might constrain the *n*-alkyl chain packing. However, small variations of ^{14}N and ^{81}Br NMR parameters are observed as a function of the chain length. These variations are mostly related to small differences in C−N−C angles and in spatial distributions of cations and anions. Moreover, it was found that ^{14}N and ^{81}Br nuclei appear to be very sensitive NMR probes to monitor the local site geometries of the polar head groups and their respective counteranions.

Further application of ^{14}N and ^{81}Br nuclei together with theoretical calculations for the characterization of other crystals, or more complex interfaces, e.g., in mesoporous materials, may be feasible in the very near future and is now in progress.

Acknowledgment. We gratefully acknowledge Christel Gervais (LCMC, Paris) for her first trials on HTAB calculations and Emmanuel Véron (CEMHTI, Orléans) for his support in XRD. Région Centre, Région Languedoc-Roussillon, and CNRS are acknowledged for the funding of the NMR equipments.

Supporting Information Available: HTAB polymorph III crystal structure, comprising more experimental details and data such as the atomic coordinates, and complementary ^{81}Br spectra and models for DTAB, TTAB, and OTAB. This material is available free of charge via the Internet at http://pubs.acs.org.

References and Notes

(1) Clint, J. H. *Surfactant aggregation*; Blackie and son, Chapman and Hall: Glasgow, Scotland, 1992.
(2) Porter, M. R. *Handbook of surfactants*, 2nd ed.; Blackie Academic and Professional, Chapman and Hall: Glasgow, Scotland, 1994.
(3) Chiola, V.; Ritsko, J. E.; Vanderpool, C. D. Process for producing low-bulk density silica; Office, U. P., Ed. USA, 1971; Vol. US Patent 3,556,725.
(4) Kresge, C. T.; Leonowicz, M. E.; Roth, W. J.; Vartuli, J. C.; Beck, J. S. *Nature* **1992**, *359*, 710.
(5) Corma, A. *Chem. Rev.* **1997**, *97*, 2373.
(6) Davis, M. E. *Nature* **2002**, *417*, 813.
(7) Soler-Illia, G. J. A. A.; Sanchez, C.; Lebeau, B.; Patarin, J. *Chem. Rev.* **2002**, *102*, 4093.
(8) Hamley, I. W. *Angew. Chem., Int. Ed.* **2003**, *42*, 1692.
(9) Wan, Y.; Zhao, D. *Chem. Rev.* **2007**, *107*, 2821.
(10) Monnier, A.; Schuth, F.; Huo, Q.; Kumar, D.; Margolese, D.; Maxwell, R. S.; Stucky, G. D.; Krishnamurty, M.; Petroff, P.; Firouzi, A.; Janicke, M.; Chmelka, B. F. *Science* **1993**, *261*, 1299.
(11) Huo, Q.; Margolese, D. I.; Ciesla, U.; Feng, P.; Gier, T. E.; Sieger, P.; Leon, R.; Petroff, P. M.; Schüth, F.; Stucky, G. D. *Nature* **1994**, *368*, 317.
(12) Firouzi, A.; Kumar, D.; Bull, L. M.; Besier, T.; Sieger, P.; Huo, Q.; Walker, S. A.; Zasadzinski, J. A.; Glinka, C.; Nicol, J.; Margolese, D.; Stucky, G. D.; Chmelka, B. F. *Science* **1995**, *267*, 1138.
(13) Galarneau, A.; DiRenzo, F.; Fajula, F.; Mollo, L.; Fubini, B.; Ottaviani, M. F. *J. Colloid Interface Sci.* **1998**, *201*, 105.
(14) Frasch, J.; Lebeau, B.; Soulard, M.; Patarin, J.; Zana, R. *Langmuir* **2000**, *16*, 9049.

(15) Tolbert, S. H.; Landry, C. C.; Stucky, G. D.; Chmelka, B. F.; Norby, P.; Hanson, J. C.; Monnier, A. *Chem. Mater.* **2001**, *13*, 2247.
(16) Echchahed, B.; Morin, M.; Blais, S.; Badiei, A.-R.; Berhault, G.; Bonneviot, L. *Microporous Mesoporous Mater.* **2001**, *44*−*45*, 53.
(17) Sadasivan, S.; Fowler, C. E.; Khushalani, D.; Mann, S. *Angew. Chem., Int. Ed.* **2002**, *41*, 2151.
(18) Che, S.; Lim, S.; Kaneda, M.; Yoshitake, H.; Terasaki, O.; Tatsumi, T. *J. Am. Chem. Soc.* **2002**, *124*, 13962.
(19) Blume, A.; Zemb, T. *Curr. Opin. Colloid Interface Sci.* **2002**, *7*, 66.
(20) Gov, N.; Borukhov, I.; Goldfarb, D. *Langmuir* **2006**, *22*, 605.
(21) Chen, C.-Y.; Burkett, S. L.; Li, H.-X.; Davis, M. E. *Microporous Mater.* **1993**, *2*, 27.
(22) Steel, A.; Carr, S. W.; Anderson, M. W. *J. Chem. Soc., Chem. Commun.* **1994**, 1571.
(23) Egger, C. C.; Anderson, M. W.; Tiddy, G. J. T.; Casci, J. L. Understanding the growth mechanism in SBA-1 synthesis. In *Studies in Surface Science and Catalysis*; vanSteen, E., Callanan, L. H., Claeys, M., Eds.; Elsevier: Amsterdam, 2004; Vol. 154; p 489.
(24) Melnyk, I. V.; Zub, Y. L.; Véron, E.; Massiot, D.; Cacciaguerra, T.; Alonso, B. *J. Mater. Chem.* **2008**, *18*, 1368.
(25) Jeschke, G.; Jansen, M. *Angew. Chem., Int. Ed.* **1998**, *37*, 1282.
(26) Khitrin, A. K.; Fung, B. M. *J. Chem. Phys.* **1999**, *111*, 8963.
(27) Jakobsen, H. J.; Bildsøe, H.; Skibsted, J.; Giavani, T. *J. Am. Chem. Soc.* **2001**, *123*, 5098.
(28) Grey, C. P.; Veeman, W. S. *Chem. Phys. Lett.* **1992**, *192*, 379.
(29) Grey, C. P.; Veeman, W. S.; Vega, A. J. *J. Chem. Phys.* **1993**, *98*, 7711.
(30) Sachleben, J. R.; Beverwyk, P.; Frydman, L. *J. Magn. Reson.* **2000**, *144*, 330.
(31) Hughes, E.; Gullion, T.; Goldbourt, A.; Vega, S.; Vega, A. J. *J. Magn. Reson.* **2002**, *156*, 230.
(32) Gan, Z. *J. Am. Chem. Soc.* **2006**, *128*, 6040.
(33) Cavadini, S.; Lupulescu, A.; Antonijevic, S.; Bodenhausen, G. *J. Am. Chem. Soc.* **2006**, *128*, 7706.
(34) Amoureux, J.-P.; Wang, Q.; Hu, B.; Lafon, O.; Trébosc, J.; Deng, F. *Chem. Commun.* **2008**, 6525.
(35) Bloom, M.; LeGros, M. A. *Can. J. Phys.* **1986**, 1522.
(36) Tycko, R.; Opella, S. J. *J. Am. Chem. Soc.* **1986**, *108*, 3531.
(37) Tycko, R.; Stewart, P. L.; Opella, S. J. *J. Am. Chem. Soc.* **1986**, *108*, 5419.
(38) Giavani, T.; Johannsen, K.; Jacobsen, C. J. H.; Blom, N.; Bildsøe, H.; Skibsted, J.; Jakobsen, H. J. *Solid State Nucl. Magn. Reson.* **2003**, *24*, 218.
(39) Jakobsen, H. J.; Hove, A. R.; Hazell, R. G.; Bildsøe, H.; Skibsted, J. *Magn. Reson. Chem.* **2006**, *44*, 348.
(40) Rothgeb, T. M.; Oldfield, E. *J. Biol. Chem.* **1981**, *256*, 6004.
(41) Pratum, T. K.; Klein, M. P. *J. Magn. Reson.* **1983**, *53*, 473.
(42) Bryce, D. L.; Sward, G. D. *Magn. Reson. Chem.* **2006**, *44*, 409.
(43) Gan, Z. H.; Gor'kov, P.; Cross, T. A.; Samoson, A.; Massiot, D. *J. Am. Chem. Soc.* **2002**, *124*, 5634.
(44) Jakobsen, H. J.; Hove, A. R.; Bildsøe, H.; Skibsted, J.; Brorson, M. *J. Magn. Reson.* **2007**, *185*, 159.
(45) Paradies, H. H.; Clancy, S. F. *Rigaku J.* **2000**, *17*, 20.
(46) Harris, R. K.; Becker, E. D.; CabralDeMenezes, S. M.; Granger, P.; Hoffman, R. E.; Zilm, K. W. *Pure Appl. Chem.* **2008**, *80*, 59.
(47) Fernandez, C.; Bodart, P.; Amoureux, J. P. *Solid State Nucl. Magn. Reson.* **1994**, *3*, 79.
(48) Skibsted, J.; Nielsen, N. C.; Bildsøe, H.; Jakobsen, H. J. *J. Am. Chem. Soc.* **1993**, *115*, 7351.
(49) Hayashi, S. *Magn. Reson. Chem.* **1996**, *34*, 791.
(50) Massiot, D.; Fayon, F.; Capron, M.; King, I.; Calvé, S. L.; Alonso, B.; Durand, J.-O.; Bujoli, B.; Gan, Z.; Hoatson, G. *Magn. Reson. Chem.* **2002**, *40*, 70.
(51) http://crmht-europe.cnrs-orleans.fr/dmfit/help/.
(52) Vosegaard, T.; Skibsted, J.; Bildsøe, H.; Jakobsen, H. J. *J. Phys. Chem.* **1995**, *99*, 10731.
(53) Cadars, S.; Lesage, A.; Hedin, N.; Chmelka, B. F.; Emsley, L. *J. Phys. Chem. B* **2006**, *110*, 16982.
(54) Pham, T. N.; Griffin, J. M.; Masiero, S.; Lena, S.; Gottarelli, G.; Hodgkinson, P.; Filip, C.; Brown, S. P. *Phys. Chem. Chem. Phys.* **2007**, *9*, 3416.
(55) Hiet, J.; Deschamps, M.; Pellerin, N.; Fayon, F.; Massiot, D. *Phys. Chem. Chem. Phys.* [Online early access]. DOI: 10.1039/B906399D. Published Online: June 26, **2009**.
(56) Saunders, V. R.; Dovesi, R.; Roetti, C.; Orlando, R.; Zicovich-Wilson, C. M.; Pascale, F. N. M.; Civalleri, B.; Doll, K.; Harrison, N. M.; Bush, I. J.; D'Arco, P.; Llunell, M. *CRYSTAL 06 user's manual*; Universita' degli Studi di Torino: Torino, Italy, 2008.
(57) Wyckoff, R. W. G. *Crystal Structures*, 2nd ed.; Interscience, John Wiley and Sons: New York, 1965; Vol. 1.
(58) Dufourcq, J.; Haget-Bouillaud, Y.; Chanh, N. B.; Lemanceau, B. *Acta Crystallogr.* **1972**, *B28*, 1305.
(59) Evans, D. J.; Hughes, D. L. *Acta Crystallogr.* **1990**, *C46*, 1452.
(60) Becke, A. D. *J. Chem. Phys.* **1993**, *98*, 5648.
(61) Lee, C.; Yang, W.; Parr, R. G. *Phys. Rev. B* **1988**, *37*, 785.
(62) Gatti, C.; Saunders, V. R.; Roetti, C. *J. Chem. Phys.* **1994**, *101*, 10686.
(63) http://www.crystal.unito.it/Basis_Sets/Ptable.html.
(64) Godbout, N.; Salahub, D. R.; Andzelm, J.; Wimmer, E. *Can. J. Chem.* **1992**, *70*, 560.
(65) Frisch, M. J.; Trucks, G. W.; Schlegel, H. B.; Scuseria, G. E.; Robb, M. A.; Cheeseman, J. R.; Montgomery, J. A., Jr.; Vreven, T.; Kudin, K. N.; Burant, J. C.; Millam, J. M.; Iyengar, S. S.; Tomasi, J.; Barone, V.; Mennucci, B.; Cossi, M.; Scalmani, G.; Rega, N.; Petersson, G. A.; Nakatsuji, H.; Hada, M.; Ehara, M.; Toyota, K.; Fukuda, R.; Hasegawa, J.; Ishida, M.; Nakajima, T.; Honda, Y.; Kitao, O.; Nakai, H.; Klene, M.; Li, X.; Knox, J. E.; Hratchian, H. P.; Cross, J. B.; Adamo, C.; Jaramillo, J.; Gomperts, R.; Stratmann, R. E.; Yazyev, O.; Austin, A. J.; Cammi, R.; Pomelli, C.; Ochterski, J. W.; Ayala, P. Y.; Morokuma, K.; Voth, G. A.; Salvador, P.; Dannenberg, J. J.; Zakrzewski, V. G.; Dapprich, S.; Daniels, A. D.; Strain, M. C.; Farkas, O.; Malick, D. K.; Rabuck, A. D.; Raghavachari, K.; Foresman, J. B.; Ortiz, J. V.; Cui, Q.; Baboul, A. G.; Clifford, S.; Cioslowski, J.; Stefanov, B. B.; Liu, G.; Liashenko, A.; Piskorz, P.; Komaromi, I.; Martin, R. L.; Fox, D. J.; Keith, T.; Al-Laham, M. A.; Peng, C. Y.; Nanayakkara, A.; Challacombe, M.; Gill, P. M. W.; Johnson, B.; Chen, W.; Wong, M. W.; Gonzalez, C.; Pople, J. A. *Gaussian 03*, revision C.02; Gaussian, Inc.: Pittsburgh, PA, 2003.
(66) Krishnan, R.; Binkley, J. S.; Seeger, R.; Pople, J. A. *J. Chem. Phys.* **1980**, *72*, 650.
(67) Curtiss, L. A.; McGrath, M. P.; Blandeau, J.-P.; Davis, N. E.; Binning, R. C., Jr.; Radom, L. *J. Chem. Phys.* **1995**, *103*, 6104.
(68) Glukhovstev, M. N.; Pross, A.; McGrath, M. P.; Radom, L. *J. Chem. Phys.* **1995**, *103*, 1878.
(69) Kutzelnigg, W.; Fleischer, U.; Schindler, M. *Al - Cl: The IGLO-Method: Ab Initio, Calculation and Interpretation of NMR Chemical Shifts and Magnetic Susceptibilities*; Springer-Verlag: Heidelberg, Germany, 1990; Vol. 23.
(70) Dunning, T. H., Jr. *J. Chem. Phys.* **1989**, *90*, 1007.
(71) Woon, D. E.; Dunning, T. H., Jr. *J. Chem. Phys.* **1993**, *98*, 1358.
(72) Harris, R. K.; Becker, E. D.; Cabral-De-Menezes, S. M.; Goodfellow, R.; Granger, P. *Pure Appl. Chem.* **2001**, *73*, 1795.
(73) *The hydrophobic effect*; Tanford, C., Ed.; Wiley: New York, 1980.
(74) *Chem3D Pro 11.0.1*; CambridgeSoft: Cambridge, MA, 2007.
(75) Bastow, T.; Massiot, D.; Coutures, J. P. *Solid State Nucl. Magn. Reson.* **1998**, *10*, 241.
(76) The same value is obtained for HTAB by $^{15}N\{^{1}H\}$.
(77) Other spectra and models are accessible as Supporting Information.
(78) Walter, T. H.; Turner, G. L.; Oldfield, E. *J. Magn. Reson.* **1988**, *76*, 106.
(79) Blanchard, J.; Bonhomme, C.; Maquet, J.; Sanchez, C. *J. Mater. Chem.* **1998**, *8*, 985.
(80) Alavi, A.; Lynden-Bell, R. M.; Willis, P. A.; Swainson, I. P.; Brown, R. J. C. *Can. J. Chem.* **1998**, *76*, 1581.
(81) Norbert, A.; Brun, B.; Dara, C. *Bull. Soc. Fr. Mineral. Crystallogr.* **1975**, *98*, 111.
(82) Szulzewsky, K.; Schulz, B.; Vollhardt, D. *Cryst. Res. Technol.* **1983**, *18*, 1003.
(83) Campanelli, A. R.; Scaramuzza, L. *Acta Crystallogr.* **1986**, *C42*, 1380.
(84) Ramos-Silva, M.; Matos-Beja, A.; Paixão, J. A. *Acta Crystallogr.* **2003**, *E59*, o1151.
(85) Johnson, C.; Moore, E. A.; Mortimer, M. *Solid State Nucl. Magn. Reson.* **2005**, *27*, 155.
(86) Thangaraj, A.; Rajamohanan, P. R.; Suryavanshi, P. M.; Ganapathy, S. *J. Chem. Soc., Chem. Commun.* **1991**, 493.
(87) Blears, D. J.; Danyluk, S. S.; Bock, E. *J. Phys. Chem.* **1968**, *72*, 2269.
(88) Dufourcq, J.; Lemanceau, B. *J. Chim. Phys.* **1970**, *67*, 9.
(89) Mahajan, M.; NageswaraRao, B. D. *J. Phys. Chem. Solids* **1972**, *33*, 2191.
(90) Albert, S.; Gutowsky, H. S.; Ripmeester, J. A. *J. Chem. Phys.* **1972**, *56*, 3672.
(91) Polak, M.; Sheinblatt, M. *J. Magn. Reson.* **1973**, *12*, 261.
(92) Ratcliffe, C. I.; Ripmeester, J. A. *Can. J. Chem.* **1986**, *64*, 1348.
(93) The modeling of rotations and their effect on C_Q is not simple to estimate. A more complex combination of both C_3 and C_2 rotations may also exist. Moreover, bond lengths and angles which define the TMA^+ cation at low temperature may change significantly at ambient temperature, leading to significant modifications in C_Q.
(94) Henriksson, U.; Blackmore, E. S.; Tiddy, G. J. T.; Soederman, O. *J. Phys. Chem.* **1992**, *96*, 3894.
(95) This correlation is not valid for NH_4Cl, but in this case, N atoms are directly bound to H atoms and not to C atoms.
(96) Trill, H.; Eckert, H.; Srdanov, V. I. *J. Phys. Chem. B* **2003**, *107*, 8779.

JP9027904